Volume 2 | Issue 2 | 2020

Official Publication

Association of Energy Engineers

Volume 2 | Issue 2 | 2020

Alternative Energy & Distributed Generation Journal

Alternative Energy & Distributed Generation Journal

AREDI ALTERNATIVE & RENEWABLE ENERGY DEVELOPMENT INSTITUTE

Cogeneration & Distributed Generation Institue

ISSN: 2643-6973 (Print)
ISSN: 2643-6981 (Online)

Editor **Jorge B. Wong Kcomt**
PhD, PE, CEM

Alternative Energy and Distributed Generation Journal

Jorge B. Wong Kcomt, PhD, PE, CEM, Editor-in-Chief
Dr. Ing. Jose Ramos Saravia, Associate Editor

Vol. 2, No. 2—2020

Contents

JOURNAL OF THE ASSOCIATION OF ENERGY ENGINEERS®

ISSN: 2643-6973 (print)
ISSN: 2643-6981 (on-line)

AREDI ALTERNATIVE & RENEWABLE ENERGY DEVELOPMENT INSTITUTE

Dr. Ing. Jorge B. Wong Kcomt
Editor-in-Chief
WK Engineers, USA
jwong@aeecenter.org

Dr. Ing. José Ramos-Saravia
Associate Editor
Dept. of Energy Engineering UTEC-Peru
ramos.jose.cesar@gmail.com

Distributed Generation And Alternative Energy Journal (ISSN 2643-6981) is published bimonthy by the Association of Energy Engineers, 3168 Mercer University Drive, Atlanta, GA 30341. Production Office: 3168 Mercer University Drive, Atlanta, Ga. 30341, 770-447-5083, ext. 224.

Subscriptions: $439 for individual print subscriptions; $548 for combined print and online subscriptions; $466 for online only subscriptions. Print only institutional subscriptions are not available.

AEE MEMBERSHIP CHANGES

Please notify Association of Energy Engineers, 3168 Mercer University Drive,
Atlanta, GA 30341
Tel: 770-447-5083, ext. 224, email membership@aeecenter.org.

EDITORIAL OFFICE

Articles and letters to the editor should be submitted to Jorge B. Wong Kcomt, Editor, Alternative Energy and Distributed Generation Journal, Email: jwong@aeecenter.org.

Publication Policy

Alternative Energy and Distributed Generation Journal is a peer-to-peer communication channel for practicing energy managers. Thus, all articles must be of a practical nature and should not be pure or basic research. If the article appears to be basic research oriented, the author(s) must explain in a leading paragraph why practicing energy managers should know the material.

Peer review is offered if requested by the author(s), but peer review must be requested in the submission email or letter. This will add about 6 months to the lead time before publishing. All other articles will be editor reviewed.

Transfer of copyright to AEE must occur upon submission and if any of the material has been published in other journals previously, that source must be identified and referenced. If the previous publication was at an AEE conference or in another AEE publication, that should also be referenced. All articles appearing in the journal are opinions and works of the authors and not AEE or the editor.

If you are submitting an article for possible publication you hereby grant AEE the right to print and assign a release of copyright of submitted article to AEE. If you are submitting an article under a governmental agency and submitted work is covered in the public domain, you hereby grant to AEE the right to reprint submitted work.

The Wuhan Virus Has Changed Everything

> The only viable endgame is to play whack-a-mole with the new coronavirus, suppressing it until a vaccine can be produced. With luck, that will take 18 to 24 months. During that time, new outbreaks will probably arise. Much about that period is unclear, but the dozens of experts whom I have interviewed agree that life as most people knew it cannot fully return. "I think people haven't understood that this isn't about the next couple of weeks," said Michael Osterholm, an infectious-disease epidemiologist at the University of Minnesota. "This is about the next two years."
>
> —Ed Yong of *The Atlantic*, as cited in *The New York Times* by David Leanhardt[i]

This virus from Wuhan, China, is a very nasty one, indeed. As "nasty" says, "nasty" does—#45 POTUS D.J. Trump. But that's a different story. The US is paying in lives, livelihoods, health sequels, money and prestige due to the sheer incompetence of the White House's tenant. But he can't help himself. He is only true to his abject nature.

What can I do? There is plenty of time to do things I thought I didn't have time to, before. While in lockdown, I can read more, learn music, build and repair things in my workshop, exercise—indoors when in town and outdoors when I am at my organic banana farm. In Peru, I have the privilege to go out because I produce food. But I am also teaching classes online, helping my town civil defense team, and writing. *See map below of my home town, Chepén, Peru.*

Let's look back at what Bill Gates said in a TED Talk[ii]. If you haven't watched it, you must. And read his report about it[iii]. He warned the world in 2015 about the NEXT EPIDEMIC:

> ***What I've learned is very sobering. As awful as this epidemic has been, the next one (this one) could be much worse. The world is simply not prepared to deal with a disease—an especially virulent flu, for example—that infects large numbers of people very quickly. Of all the things that could kill 10 million people or more, by far the most likely is an epidemic.***

What We Must Do Now: TEST MORE, TEST BETTER

And now we need to prioritize test capacity. Rapid testing to identify and focus on geographical areas or human groups with high (or potentially high)

---

i https://www.nytimes.com/2020/04/16/opinion/coronavirus-reopen-economy-singapore.html
ii https://www.youtube.com/watch?v=6Af6b_wyiwI
iii https://www.gatesnotes.com/Health/We-Are-Not-Ready-for-the-Next-Epidemic

infection incidence. And use the more accurate molecular tests to diagnose and treat patients. It's not only that we need to test more, but better. To test better, we need a system or process using all means necessary, people, digital and media based, to track and find suspect cases and follow up with isolation and treatment, relentlessly. Every infected and suspect person deserves to be helped and to hear an empathetic human voice. To carry out and support such a mission, we need a task force of trained people from each country's armed forces reserves. The support of independent health professionals (from doctors to EMTs, from nurses to undertakers) is VITAL too. Having a standardized process to carry out such a mission is paramount to train well the task force, to supervise and evaluate progress, to detect and solve problems and to improve continually.

Chepen is a province of the Jequetepeque Valley. The county seat, the town of Chepen is the blue dot in the maps shown below. The town is nestled in the foothills of the Northern Peru Andes mountains. The Jequetepeque River runs from east to west and opens onto a wide delta of rice fields. The Pacific Ocean is on the left. Our weather is similar to Southern California's. Come to visit, when the pandemic is gone.

Endnotes

1 https://www.youtube.com/watch?v=6Af6b_wyiwI

2 https://www.gatesnotes.com/Health/We-Are-Not-Ready-for-the-Next-Epidemic

Harvesting Heat Energy as Alternative Renewable Energy

M.K. Chan, J.M.Y. Lim†, P. Kumaran**

ABSTRACT

Research on renewable energy is on-going due to the desire to create a better living environment and to secure energy supply to the world. Existing research uses thermoelectric generators (TEG) to generate renewable energy. In this research, instead of using TEG, the use of thermoelectric cooler (TEC) to power up a lab scale car (TECar) is disclosed for the first time in this article. Results show that the heat generated from chemical reaction can be converted into electricity with the use of TEC and voltage booster, creating renewable energy. The generated voltage from TEC and voltage booster is approximately 30V, which is enough to power up the lab scale car without the use of any other power source. In conclusion, the idea of using TEC to convert heat energy into electricity, to power up a lab scale car is shown. Moving forward, TEC can be installed at the hot surface of a car's engine compartment to generate electricity, creating renewable energy.

Keywords: Thermoelectric Cooler, Green car, Renewable energy.

INTRODUCTION

Rapid development of renewable energy resources and its technological diversification results in energy security and economic benefits. Some of the existing renewable energy includes rain, wind, sunlight, rain, waves, and geothermal heat. The usage of heat to electricity had been studied by (Yang and

---

*Centre for Advanced Electrical and Electronic Systems, Faculty of Engineering and the Built Environment, SEGi University, Jalan Teknologi, Kota Damansara, 47810 Petaling Jaya, Selangor, Malaysia.

†Electrical and Computer Systems Engineering, School of Engineering, Monash University, Subang Jaya, Malaysia.

Liu, 2010) by using thermoelectric generator (TEG). In this article, a cheaper alternative is explored where thermoelectric cooler (TEC) is used to harvest heat and convert it to electricity, reducing global warming.

The main contributions of this research work are as follow s: Firstly, TEC is used with voltage booster to generate electricity, enough to power up a lab scale car without the use of other power sources. Secondly, TEC is shown to incur lower cost in terms of energy supply as compared to battery or TEG. Thirdly, harvesting heat from car engine to create electricity, with the use of TEC, results in significant increase of energy efficiency.

The rest of the article is organized as follows. Section 2 illustrates the existing work. Section 3 discusses the proposed TECar. Section 4 presents and discusses the experimental and analytical results. Section 5 concludes the article.

LITERATURE SURVEY

Efforts to minimize the dependence on petroleum as the main energy source to reduce greenhouse gas emissions are attempted by researchers in the past few decades. Many alternative methods are explored in creating efficient renewable energy.

One of the renewable energy technologies for cars includes powering up a car with the use of biofuel from biomass. Producing biofuel from biomass gains a lot of attention from the researchers and investors as it uses waste feedstock as the raw material and this secures energy supply. In Brazil, approximately 3.14 million metric tonne of sugarcane was used to produce bio ethanol in the year 2014 (Barros, 2014) where complicated biological or chemical treatments and processes were required for the production. However, it was shown that the type of biomass, gasification techniques, operating condition (Andersson, 2015) and choice of catalyst (He and Zhang, 2008) are important for converting syngas gas to ethanol via thermo-chemical method. Additionally, limited waste feedstock supply may also affect the supply of biofuel (Sims et al., 2008).

Fuel cell is another type of renewable energy technology that has been explored by the researchers (Roshandel et al., 2015; Benaissa et al., 2014; Li et al., 2011). Fuel cells convert chemical energy to electricity, via the reaction between hydrogen and oxygen. It is claimed as green technology as it produces only water as the end product. Several fuel cell cars such as Toyota Mirai are Hyundai ix35 are readily available in the market. However, the hydrogen gas tanks have to be delivered to the respective petrol station for the users to refill hydrogen where high carbon footprint is incurred, as big trucks are required for the gas tanks delivery.

Alternatively, hybrid cars are also widely used as one of the renewable energy efforts to ensure efficient energy. Hybrid cars operate with two sources of energies, which are battery and petrol, enabling them to offer better fuel economy and fewer emissions. Typical hybrid cars operate with an on-board sensor that captures upcoming trip data to optimally adjust the vehicle's speed, results in high energy efficiency (Vajedi and Azad, 2016). Hybrid cars can be modelled with enhanced system configuration to improve its reliability (Rieker et al., 2015). However, hybrid cars are costly in the long run due to expensive batteries and switching equipment.

While the aforementioned literature laid a solid foundation in car's renewable energy, harvesting heat from the car's engine with the use of TEC and voltage booster has yet to be explored. TEC is a device that converts heat energy to electricity when a temperature difference between the heat and cold sides is found. This article discusses the practicality of using TEC to power up a lab scale car. The performance of a lab scale car is measured by its velocity.

EXPERIMENTAL SETUP

Thermoelectric Cooler with Voltage Booster Powered Lab Scale Car (TECar)

In the proposed TECar, a TEC is placed between the heat source and ice, as shown in Figure 1. The heat was supplied by the exothermic reaction between hydrochloric acid and aluminium. A voltage booster is connected to the TEC and then to the motor. The container is used to carry loads. The generated voltage is measured by using a voltmeter whereas thermometer is used to measure the temperature of the mixture of chemical solution and ice. The performance of the car is measured by the cost incurred and energy efficiency.

The proposed TECar works based on a closed loop feedback control system as shown in Figure 2, where the temperature difference (ΔT) is represented by the reference input and the power generated is represented by the controlled output. The amount of heat acts as the error detector. The TEC, voltage booster and motor acts as the comparator and the controller. The corrective signal generated is represented by the control signal, which is transmitted to TEC. The TEC and voltage booster form the actuator unit. The motor forms the process.

In order to create the temperature difference needed for TEC to generate

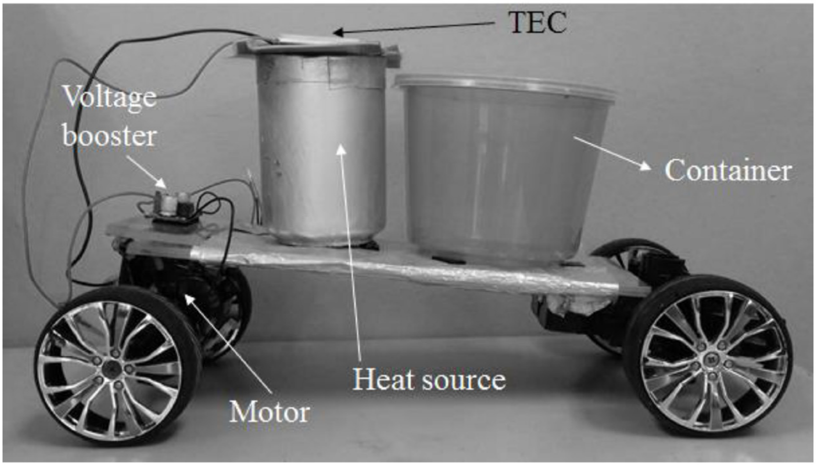

Figure 1. Lab scale TEC powered car (TECar)

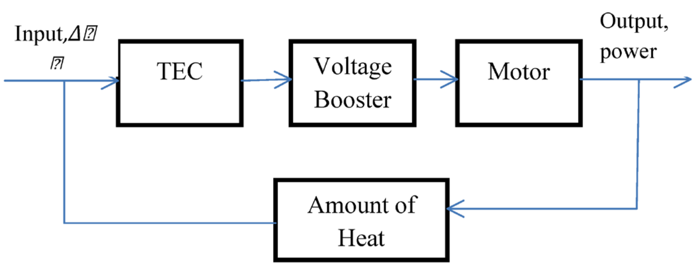

Figure 2. Closed loop feedback control system for TECar

electricity, to power up a lab scale car, the reaction between aluminium and hydrochloric acid is used to generate heat. Figure 3 shows the increment of the mass of aluminium from 1.5g to 2.5g in hydrochloric acid increases the temperature of the mixture and the voltage generated from the voltage booster. It is due to the exothermic reaction between aluminium and hydrochloric acid, and the higher temperature difference causes higher voltage generated from the TEC-voltage booster device. However, further increase in the mass of aluminium does not increase the voltage significantly. It shows the maximum capacity of the TEC-voltage booster device is to generate 10~30V with 0.01~0.1A.

Table 1 shows the effect of loads carried by the car have on the velocity of the car. When the load increases 200% of the initial loads (48.2662g), the

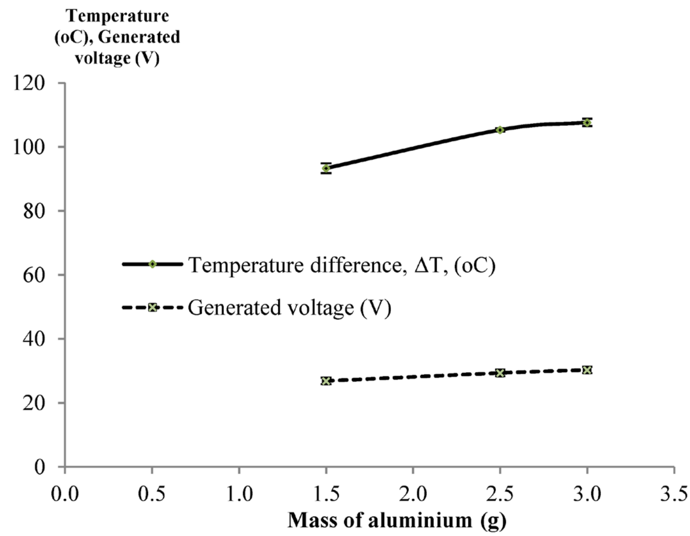

Figure 3. Effect of the mass of aluminium in hydrochloric acid on the temperature different across the TEC and the generated voltage

Table 1. The performance of the car in terms of velocity

Loads carried by the car (g)	Velocity (m/s)
0.0000	0.2369 ± 0.0316
48.2662	0.2069 ± 0.0153
96.5323	0.1945 ± 0.0098
144.7985	0.1418 ± 0.0087

velocity of the car only reduces 31% from its initial velocity. It shows that this method of harvesting and converting heat energy to electricity works and it can supply energy to a heavier car.

The findings here prove that TEC can be used to produce electricity to power a lab scale car. According to Fairchild et al. (2002), the temperature of the engine surface and exhaust system are 140°C and 587°C respectively. Heat generated from this engine compartment can be used as the heat source for the TEC to generate electricity. Meanwhile, the cold side of the TEC can be exposed to the air flow. This temperature difference causes the TEC to generate electricity, which can be used to power up the car. Moving forward, the four strokes engine could be replaced by any exothermic chemical reaction to provide heat to the TEC.

RESULT AND DISCUSSION

In order to power up a lab scale car, three energy sources are used in this experiment; TEC, battery and TEG. The experiment parameters are shown in Table 2. The percentage of cost reduction and energy efficiency are tabulated in Tables 3 and 4.

Table 2. Experiment parameters

Parameter	Value
Price of chemicals used (2.5g of aluminium and 35 ml of hydrochloride acid)	USD 3.21
Time taken to fully charge the battery	420 minutes

Table 3. Percentage of cost reduction

***Refer to supplementary material**

Power Supply	Cost (USD)	Percentage of Cost Reduction as compared to Battery
9V Rechargeable battery* + electricity charges*	13.49 + 37.80 = 51.29	-
TEG* + Chemicals*	25.30 + 3.21 = 28.51	44.41%
TEC* + Voltage Booster* + Chemicals*	21.52 + 0.48 + 3.21 = 25.21	50.85%

*Refer to supplementary material

Table 4. Energy efficiency

Power Source	Kwh Generated	Kwh after Voltage Booster	Energy Efficiency as compared to TEG
Battery (Tenergy Corporation, 2009)	9V * 0.01A = 0.000090	-	100%
TEG (David Salerno, 2010)	4.5V l* 0.01A = 0.000045	-	-
TEC (Linear Technology, 2001)	2.7V * 0.01A = 0.000027	0.00027	500%

Table 3 shows the percentage of cost reduction with the proposed TECar, as compared to battery and TEG powered lab scale cars. Using rechargeable battery to power up a lab scale car incurred a total amount of USD 51.29. Using TEG, with chemicals to create temperature difference, shows 44.41% cost reduction as compared to battery powered car. In the proposed TECar, the lab scale car is powered by TEC and voltage booster, with chemicals to create temperature difference, resulting in 50.85% cost reduction in power supply. Since TEC does not require electricity charges to run, instead it generates electricity with the use of temperature difference created by chemicals, the cost of power supply is therefore much lower than battery operated lab scale car. On the other hand, the cost of TEC with voltage booster is lower than TEG, resulting in higher cost reduction. If the TEC is installed in the car engine, with temperature difference created by the heat from the engine, the cost of chemicals can be voided, incurring even lower power supply cost.

Table 4 shows the energy efficiency of TEC powered car as compared, to battery and TEG powered car. TEG has the lowest energy efficiency; therefore it is used as the benchmark. As compared to TEG, battery powered lab scale car is shown to have 100% much higher energy efficiency. On the other hand, the proposed TECar is shown to exhibit 500% much higher energy efficiency as compared to TEG powered lab scale car. Results show that the proposed TECar shown higher cost reduction and higher energy efficiency which makes it suitable as a renewable power supply for the car industry.

CONCLUSIONS

Renewable energy shows potential to be promising solutions for energy saving and cost reduction. The idea of using TEC to convert energy for vehicle use is proven in this study. In this study, a lab scale car powered by TEC and voltage booster, TECar, is shown to reduced cost and increase energy efficiency, as compared to battery and TEG powered car. The proposed approach considers converting available unused heat source into reliable energy source to power up a lab scale car, with the used of TEC and voltage booster, creating renewable energy. In future, the idea of TECar can be implemented into different applications, to create renewable energy, for better future.

References

Andersson, R., Catalytic Conversion of Syngas to Higher Alcohols over MoS2-based Catalysts. Sweden: Royal Institute of Technology, 2015.

Barros, S., Brazil-Biofuel Annual. Technical Report BR14004. USDA Foreign Agricultural Service, Global Agricultural Information Network, United State, 2014.

Benaissa, A., Rabhi, B., Moussi, A., Aissa, D., A linear quadratic regulator control of a stand-alone PEM fuel cell power plant. Frontiers in Energy, 8(1), 62-72, 2014.

Fairchild, M.R., Snyder, R.B., Berlin, C. W. and Sarma, D.H.R., Emerging substrate technologies for harsh-environment automotive electronics applications. In: SAE 2002 World Congress. Detroit: Society of Automotive Engineers, 1-10, 2002.

Rieker, T., Zeiler, P., Bertsche, B., Reliability analysis of a hybrid car drive system with ECSPN. In: Annual Reliability and Maintainability Symposium. Florida: Institute of Electrical and Electonics Engineers, 1-7, 2015.

He, J., Zhang, W.N., Research on ethanol synthesis from syngas. Journal of Zhejiang University Science A, 9(5), 714-719, 2008.

Li, Y., Weng, Y., Weng, S., Part-load, startup, and shutdown strategies of a solid oxide fuel cell-gas turbine hybrid system. Frontiers in Energy, 5(2), 181-194, 2011.

Roshandel, R., Astaneh, M., Golzar, F., Multi-objective optimization of molten carbonate fuel cell system for reducing CO_2 emission from exhaust gases. Frontiers in Energy, 9(1), 106-114, 2015.

Salerno, D., Ultralow Voltage Energy Harvester uses Thermoelectric Generator for Battery-Free Wireless Sensors. LT Journal of Analog Innovation, 20(3), 1-11, 2010.

Sim, R., Taylor, M., Saddler, J., Mabee, W., From 1st to 2nd Generation Biofuel Technologies-An Overview of Current Industry and RD&D Activities. Technical Report IEA/OECD. International Energy Agency (IEA,) France, 2008.

Tenaga Nasional Berhad., Tarrif Book. Malaysia, 2006.

Vajedi, M., Azad, N.L., Ecological adaptive cruise controller for plug-in hybrid electric vehicles using nonlinear model predictive control. IEEE Transactions on Intelligent Transportation Systems, 17(1), 13-122, 2016.

Yang, Y., Liu, J., Evaluation of the power-generation capacity of wearable thermoelectric power generator. Frontiers of Energy and Power Engineering in China, 4(3), 346-357, 2010.

AUTHOR BIOGRAPHIES

Chan Mieow Kee received her Bachelor of Chemical Engineering (with honors) from University Technology Malaysia in 2007 and her PhD in 2011. She is currently a senior lecturer in the Department of Chemical Engineering in SEGi University.

Joanne Mun-Yee Lim received her Bachelor of Engineering (with honors) from Monash University in 2008, her Master of Engineering Degree from University Malaya in 2011, and her PhD (Engineering) from Multimedia University in 2016. She is a member of The Institution of Engineers Malaysia and a professional engineer in the Board of Engineers Malaysia. She is currently serving as a Lecturer in the Department of Electrical and Computer System Engineering, in Monash University Malaysia. Her research interest includes Vehicular Ad-hoc Network (VANET), mobile IPv6 based networks, artificial intelligence, control systems, optimization schemes, robotic design and applications.

Prasilla Kumaran is currently an undergraduate student of Bachelor of Chemical Engineering in SEGi University.

Active Filter Based Harmonic Mitigation Technique for Islanded Microgrids

Mohammad Zeeshan and Majid Jamil, Department of Electrical Engineering, Jamia Millia Islamia, Maulana Mohammad Ali Jauhar Marg, Jamia Nagar, New Delhi, 110025, India

ABSTRACT

This article delves into some aspects related to transient control of microgrid in islanded condition. A microgrid is emerging as the solution to meet the developing energy needs of society. It is a combination of interconnected distributed resources which are often interfaced with the utility grid. It can also function independently in cases of failure of the main grid, i.e. islanded condition. During progression from the grid-connected mode to the islanded operation, several mismatches take place between the source and the load which causes problems in control of voltage and frequency. Designing a proper control strategy is crucial for the maintenance of proper stability and quality of power in the microgrid setup. It has been shown that the deployment of active filters can smooth out this transition and help in reducing the harmonic distortion which may otherwise be present in the case of passive filters. A microgrid setup has been simulated in MATLAB with different distributed renewable sources and storage. Fuzzy controllers are used to establishing the islanding condition in the microgrid studied and then the islanding condition is detected and controlled.

INTRODUCTION

The electric power sector is recently facing several issues since the consumer needs are increasing gradually. The current high voltage network is lagging behind which includes improper use of resources and since the resources on

[1]Corresponding author: zee123king1@gmail.com (Mohammad Zeeshan) E-mail: mjamil@jmi.ac.in.

which these networks work are depleting, this is also posing problems in distribution networks. Most of the energy is lost in transmission and distribution in the form of heat. Hence advanced energy infrastructure should work on increased reliability and efficiency, lower cost, self-healing property and an increase in the penetration of renewable energy sources [1] [2]. Utilizing a distributed energy resource (DER) allows easy proximity between source and load. However, this comes with its own set of issues such as the problem to control these DERs which are complex and costly [3]. Hence in order to compensate for the same, the concept of microgrid comes to the rescue which combines the DERs and loads into a single unit. These sources and loads can function side by side to the grid or the island which can help satisfy the needs of customers while also providing services to the grid. Islanding is the condition in a distributed generation (DG) when a microgrid continues to function and remains in a powered state even if it is detached from the main grid [4]. The power source to the critical or essential loads is maintained uninterrupted in the situation of such an event. As soon as an islanding event happens, the sectionalizing of grid happens spontaneously and the distributed generator (DG) powers up the essential load till the main grid is coordinated. The recognition of islanding event is very crucial to the control of the stability of the microgrid. An accurate detection of the islanding event will aid in the proper functioning of the switching devices resulting in rapid stabilization of the grid from the transition event.

Islanding occurs in three steps: Island formation, Islanding operations, and Resynchronization.

Depending on the cause, an islanding event can be triggered by the presence of a fault or a maintenance event. If a fault occurs in a distribution system, there may be a small interruption in the power supply for a while and the DG disconnects from the grid and steadily recouples to the essential load. An island is formed but it may deal with the problem of disparity between the load's capacity and that supplied by the source. If the capacity of both is comparable then island formation is feasible. If the island is not formed during such condition then the faulty device is separated from the grid without supply reducing the consistency of the supply. To prevent this phenomenon, the DG is first disconnected from the main supply before island formation and then the loads are slowly reconnected to the DG [5].

In case of a maintenance activity, the interruption of portions from the grid is premeditated. The total outstanding load should be nearing the capacity of the source and if this condition is disturbed then frequency outages may occur, triggering the protective devices.

During the Islanding process, there are three cases to be considered namely load following, fault, and rejection of large loads. Whenever a load change occurs, the DG must adjust the voltage and frequency to a proper level in order to meet the load requirements.

If a defect occurs in the power generation system then through islanded condition, the faulty device needs to be sorted out and separated from the main grid before the system decays into instability. Next the distributed generators have the task of bringing the voltage and frequency of the structure to stability until the fault is cleared. When a sudden ON and OFF transition event or interruption of a bulky load from the microgrid occurs, then the distributed system should be able to synchronize the system voltage and frequency quickly. Finally, the load is transferred back to the main grid separated from the faulty devices. The normal DGs have to reconnect before resynchronization of the islanding event. The islanded area is not working for this moment. If critical loads are present in the system when the number of disruptions is too high, then reliability becomes an issue which can be improved by remote resynchronization [6].

LITERATURE REVIEW

Megha et al. [7] performed the study of harmonic suppression for a multiple resource microgrid which includes diesel generator, wind turbine, PV arrays, microturbine etc. The study includes the analysis of nonlinear harmonic loads where the microgrid works at a particular set frequency when it is at the process of sharing the frequency. A distribution static compensator (DSTATCOM) is utilized to avert the harmonic currents from reaching the diesel generator, which is then controlled.

N.S. Srivatchan et al. [8] performed the study for stability control of microgrid in an islanded condition where there is a large discernment of intermittent renewable sources. Studies are done without and with a DSTATCOM which is used to minimize the voltage dip of islanded microgrid by infusing reactive power and improve the voltage stability.

H.M.A. Antunes et al. [9] improved the power quality problem of the microgrid during low short-circuit power conditions by proposing a series active hybrid filter which is then connected to the AC microgrid. It was found to be beneficial in countering the effects of harmonics and resonance conditions at the stage of common coupling (PCC) for the grid connected as well as islanded mode. This improved the power quality of the microgrid by improving the filtering property of the passive filters.

Wang et al. [10] proposed a control strategy for the distributed generation sets which are coupled to the inverter which have the combined competency to mitigate both the harmonics and the resonance issues. Many control and damping approaches have been discussed like for bulky grid-like inductances, a load compensator was utilized including a VFI as well as VHI loop. A control platform was designed and discussed to corroborate the performance of the control loop.

C. Li et al. [11] performed a review on various islanding techniques used in the microgrid. He performed a review of various issues and performance indices prevalent in the microgrid. He studied the passive recognition methods like the degree of change of frequency, power etc. and active islanding detection methods like active frequency drift, voltage shift etc. and studied the combination of various detection techniques and studied their performance. They studied the advantages and disadvantages of the various techniques discussed in the paper.

H. Moussa et al. [12] proposed a harmonic droop control method in order to recompense the harmonic currents created by every distributed generator in order to feed the nonlinear loads and decrease the voltage alterations at the point of common coupling (PCC) at the end users separately between different DGs in a single loop. This is independent of the disparity in the line impedances present in the system. The controller is tested for a resistive as well as an inductive microgrid for its competency.

A. Eshraghi, R. Ghorbani [13] studied the case when the distributed power generation exceeds the load requirements such that a transient overload condition is obtained in the case of an islanding event. The setup was able to monitor islanding detection and conditions of overvoltage. A group of sensors is used to upsurge the consistency of the system and provide a response to the instantaneous controller.

A. Ranjbaran and M. Ebadian [14] proposed a hierarchical control system to address the issues of essential load bus voltage quality and problems related to power-sharing between resources and harmonic compensation. A primary loop containing the droop control, virtual impedance and unbalanced compensation is used while a secondary loop was utilized to restore the amplitude and frequency values of the coupling voltage to minimal values. However, this study is to be performed for a real microgrid.

Y. Han et al. [15] proposed a control structure for compensating the harmonic content as well as power sharing problems utilizing various damping techniques for voltage harmonics. A hierarchical control consisting of a primary control which includes the impedance loop, compensators etc and a secondary loop consisting of the frequency and voltage refurbishment is used. Virtual loops at the fundamental frequency are utilized to get an accurate power sharing.

Y. Gui et al. [16] proposed a coordinated control mechanism for an islanded microgrid and solve the issue of synchronization without the use of a phase locked loop system which improves the stability of the system. The storage devices upkeep the voltage and frequency of the microgrid and improve the plug and play properties since synchronization is not needed in the current scenario.

R. Haider et al. [17] discussed a passive islanding technique utilizing a Kalman filter to obtain and filter the harmonic components of the voltage at DG terminals. A residual signal is generated which is used to detect variations in the power system. A study denoted as the selective harmonic distortion is used by the Kalman filter to determine harmonic components.

Compared to the conventional techniques for harmonic reductions in the microgrids, active filters pose as an inexpensive option compared to the passive filters and other alternatives due to the low-cost components. The input signal is not attenuated and the filter is easy to tune and adjust in addition to providing isolation between individual stages and control of input and output impedance. Hence this paper tries to solve the stability issue for a multi-resource microgrid while maintaining the stability and reliability of the system.

ROLE OF ACTIVE FILTERS IN RENEWABLE SYSTEMS

There are several methods commonly used to eliminate harmonic distortion in distribution systems like microgrids namely by the use of active and passive filters. Due to the dynamic nature of distribution systems passive filters are not promoted for their use in distribution networks and they may cause resonance like conditions in the circuit. This greatly affects the stability of the microgrid system. The variations in frequency and the diversions in component properties can affect the functioning of passive filter devices. Also, the new technology has been replacing their old counterparts. The introduction of the active filters has been dynamically replacing the use of passive filters in distribution circuits. The major functioning of these circuits is the active utilization of power electronic components that reduce the distortions due to harmonic components that may be present in the system due to nonlinear loads.

Active and passive filters can be utilized by renewable energy distribution structures in order to diminish the effect of harmonic distortion. The passive filters although act as the simplest solution, yet for dynamic systems they fail to fulfill their role in harmonic mitigation. They cause a resonance effect hence affecting the stable distribution system. If the power system is affected by frequency variations and varying electronic component values then this affects the stability due to improper working of the passive filters. Hence the search for a new variant is required which can overcome these problems.

The active filters have been engaging various applications in reducing the effects of harmonic distortion. Some current components produced by nonlinear loads are reduced by using advanced power electronics to the lowest possible level.

The active filters have several benefits over their passive counterparts. They can subdue the reactive currents as well as the harmonics in currents. Active filters are free from resonance effects commonly experienced by passive filters. They work independently of the power distribution network properties.

Use of Active Filters

Active filters encompass a group of electronic filters that employ active components like amplifiers for their working. The estimator generates the reference signal for compensation which is responsible for driving the system controller.

Active filters encompass a group of electronic filters that employ active components like amplifiers for their working. The estimator generates the reference signal for compensation which is responsible for driving the system controller. The gating signals are generated by the filter which controls the power distribution circuit. A generalized power circuit can be linked in series, parallel or series-parallel conformations. The active filters require prompt switching of high currents in the power circuit of active filters. The active filter comprises the following stages: the signal conditioning stage, compensatory circuit, and the gating signal generator. The harmonics are sensed in the distribution network. The proper tuning of the reference signal is important for the proper functioning of the active filter network. The reference signal can be assessed by using vital signals including current and voltage signals so that the system can track accurate system information. These parameters can be measured by using current and voltage transformers etc. Generally, the voltage of the AC source, DC bus, and the interfacing device is measured. The load and source, DC link and compensation current variables are also sensed and measured of the active filter. Hence, based on these variables, the base signals are assessed in terms of their voltage and current levels.

The following stage comprises the extraction of the counterbalancing signal from the unsettled wave which is composed of both the fundamental as well as harmonic content. This can be approached in the time or frequency domain fashion. Frequency domain utilizes the Fourier transformation while time domain may comprise other techniques like reactive power theorem, synchronous reference frame etc.

The final phase consists of the production of the gating signal which is to be utilized for the moderation of harmonics. Various techniques of control like the hysteresis control, deadbeat, sliding mode etc. are used to control the structure of active filters. Hence, a gating signal generator is employed.

BACKGROUND AND DESIGN

A microgrid simulation setup was designed in MATLAB 2016a assimilating various resources for energy generation as well as storage, which include a solar photovoltaic power system, an integrated wind generation system, distributed generators with proper control mechanisms for islanding control establishment.

A fuzzy control mechanism was established which could provide detection of an islanding event based on predefined rule base for deciding the course of the event as shown in Figure 1 and active filter design for stabilizing the system after manifestation of an islanding event by suppressing the harmonic content of the wave.

The values like df/dt, dP/dt, and df were established as discussed by Samantaray *et al.* [18]. df/dt is treated as X1, dP/dt is assumed as X2 and df as X3.

The following fuzzy logic rules were established for islanding detection:

1. (X1== a1)&(X2== w)=> (m = m1)
2. (X1== a2)&(X2== b3)=> (m = m1)
3. (X1== a2)&(X2== w) &(X3== C1)=> (m = m1)
4. (X1== a2)&(X2== w) &(X3== C2)=> (m = m2)

A Mamdani model is used in the island detection for this microgrid with centroid defuzzification technique implemented. A value of 0.5 is provided by the FIS matrix for islanding detection and if the island is not formed then no value is sensed. The active filter design is discussed in Figure 2. The active filter consists of the signal conditioning stage, the compensation stage, and gating signal generator as discussed next.

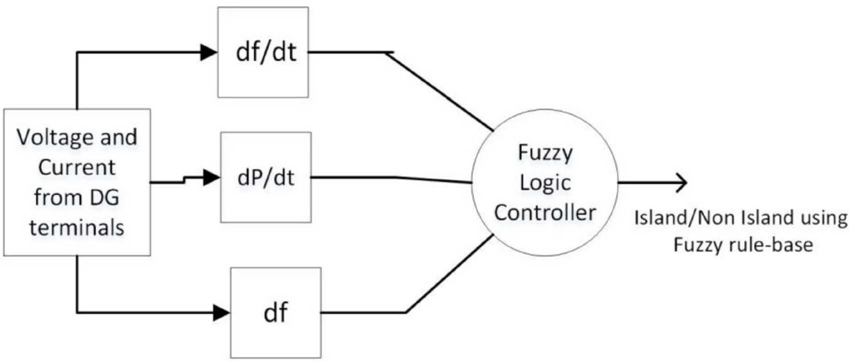

Figure 1.
Fuzzy Logic Controller establishing rule base for Island Detection

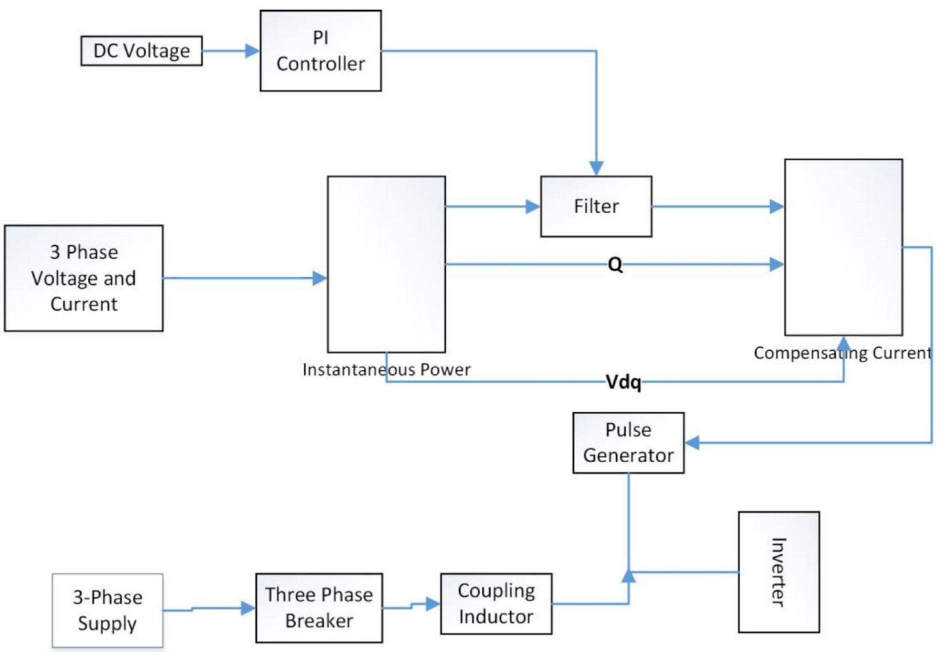

Figure 2. Active Filter Design

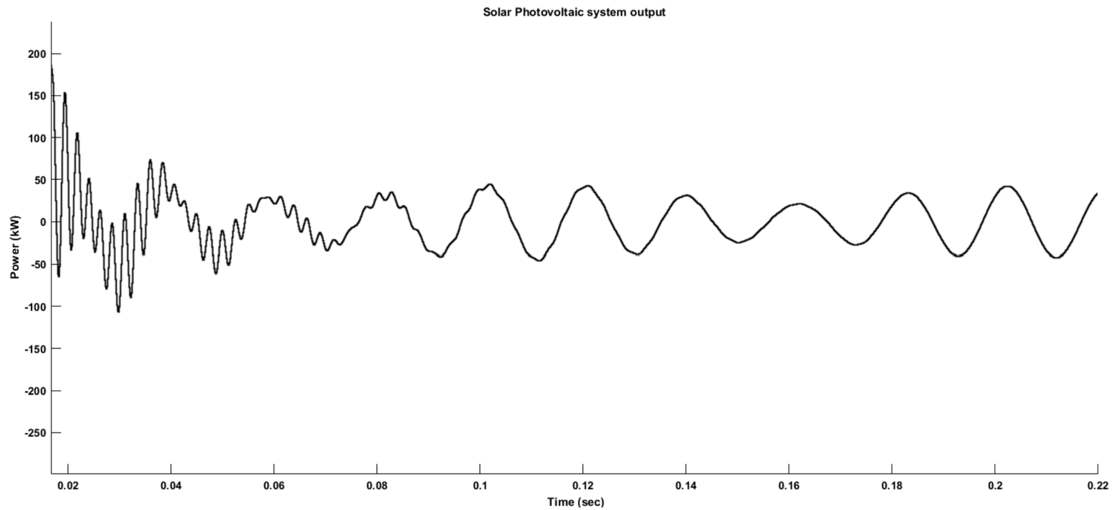

Figure 3. The occurrence of an islanding event for a solar photovoltaic system in microgrid

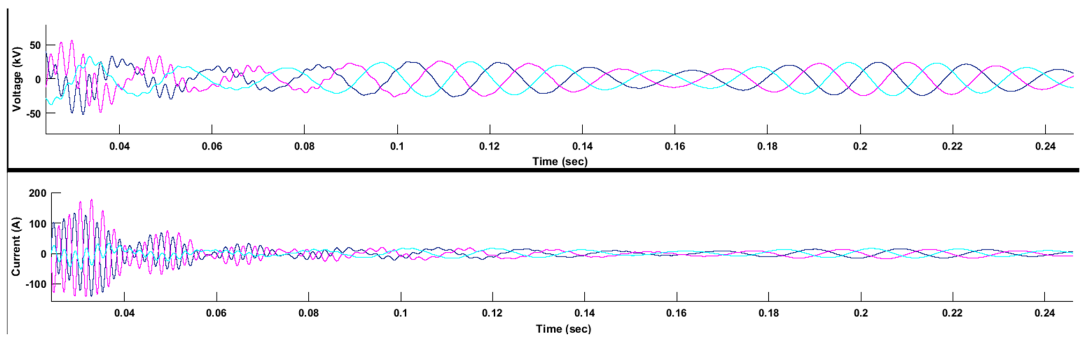

Figure 4. The occurrence of an islanding event for a wind generation system in microgrid

RESULTS

The output power of the solar photovoltaic system in the microgrid was studied. We can see that the islanding occurs at a point t = 0.017 seconds. After that time the active filter comes into operation to stabilize the microgrid and restores it from an islanding event. The active filter is composed of the PI controller which can lessen the error between the reference value V_{dc} and the obtained value. The circuit breaker of the active filter has a switching time of approximately 0.18 seconds when it becomes active and starts filtering and starts steadying the sinusoidal waves for all its components. As the islanding is detected, the input values of active filters are extracted from a bus bar on the grid. This is shown in Figure 3.

The output of the wind generation and the working of the active filter can now be studied and is depicted by Figure 4.The islanding event is fixed at 0.017 seconds. We can see the start of operation of the active filter and stabilization of the three-phase output reducing the harmonics to a minimum level.

The output of the diesel generator and the working of the active filter can now be studied and is depicted by Figure 5. The islanding event is fixed at 0.017 seconds. We can see the start of operation of the active filter and stabilization of the three-phase output reducing the harmonics to a minimum level.

The grid output can be seen in Figure 6 which depicts the starting point of the islanding event for the same switching time. The output islanding start is visualized at 0.017 seconds and the grid starts stabilizing at approximately 0.19 seconds.

The DC photovoltaic voltage drops very rapidly in the case of islanding event with time over a time event duration from 0.02 to 0.5 seconds is seen in Figure 7.

The outputs of the active filter are measured and visualized in Figure 8. The first part of the figure depicts the deviation in grid current at the event of an islanding and after stabilization, we can see changes in the load current characteristics where it reaches a peak stable value of 0.3 Amperes shown in the 2^{nd} part of Figure 8.

The magnitude of the dissimilarity depends on the variation in the load. The third part of Figure 8 depicts the characteristics of the active filter which obtains a magnitude when it comes into action stabilizing the harmonics and providing a stable output for the microgrid.

Finally, the islanding event is depicted in Figure 9 which shows that the microgrid is disengaged from the grid making its transition to the islanded state. This transition of disconnection and reconnection happens at approximately 0.017 seconds and this transition event ends at approximately 0.16 sec after which the circuit breaker of the active filter turns on and starts stabilizing the microgrid system.

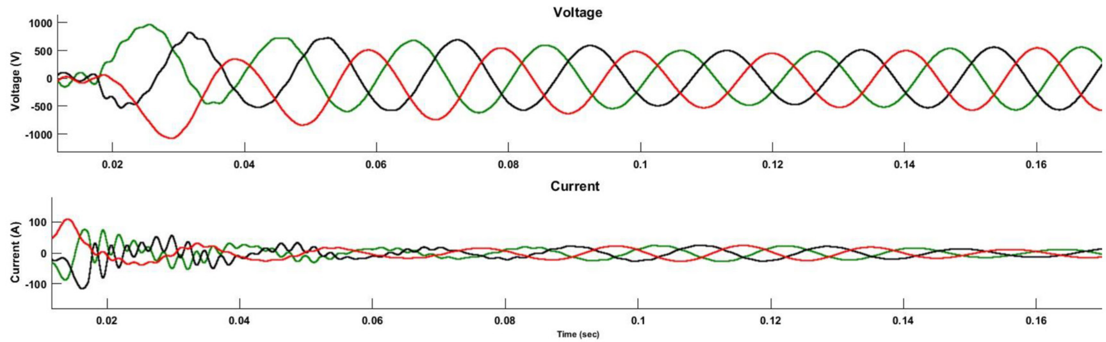

Figure 5. The occurrence of an islanding event for a diesel generator in microgrid

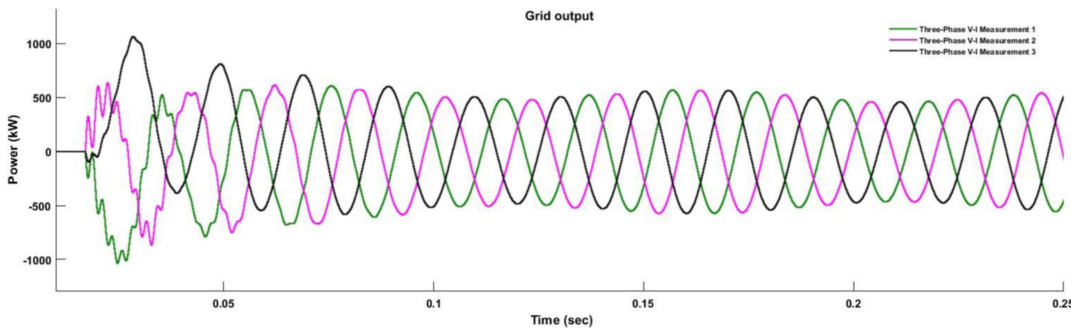

Figure 6. The occurrence of an islanding event for the grid

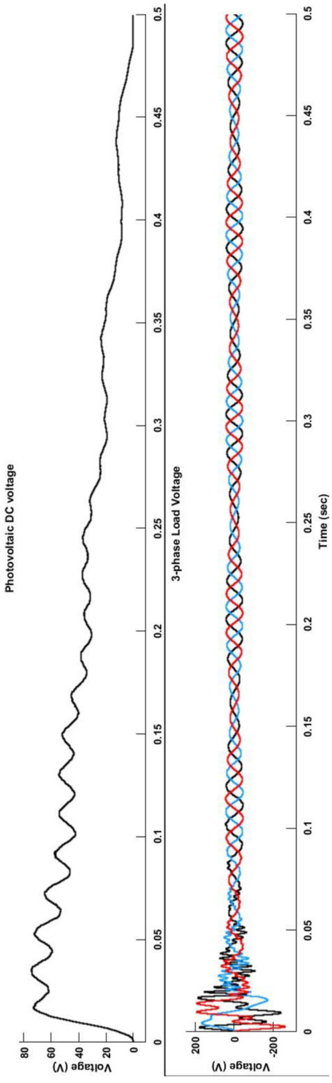

Figure 7. DC Pholtovoltaic voltage levels in islanded condition

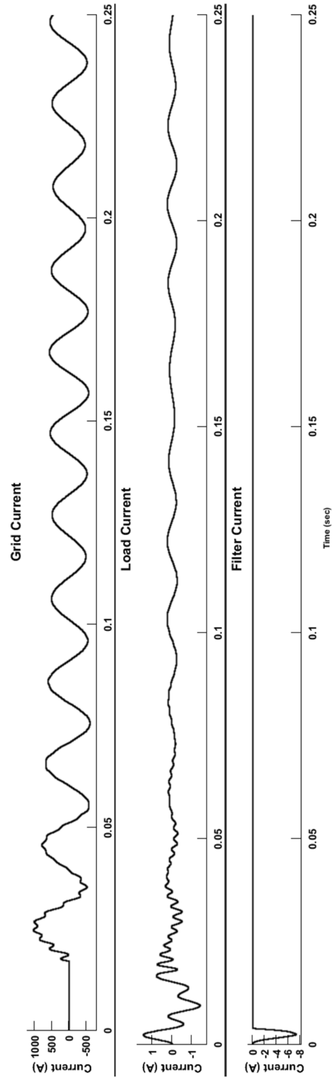

Figure 8. Variation in grid, load and active filter output at the occurrence of an islanding condition

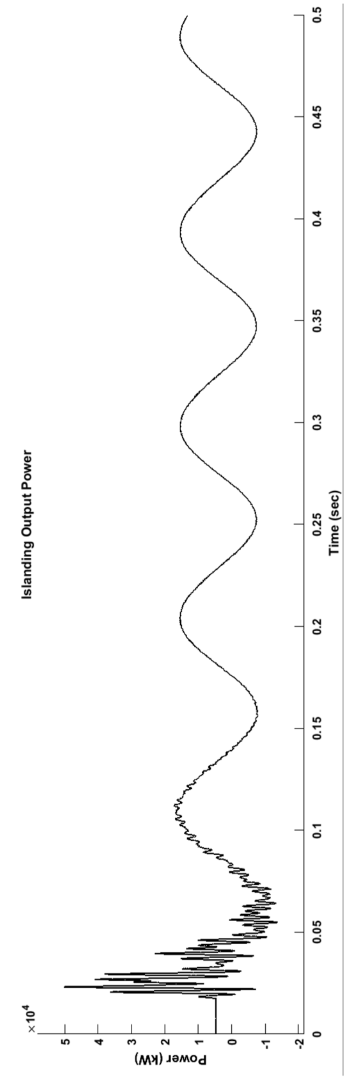

Figure 9. Islanding output power

SENSITIVITY ANALYSIS

The hybrid microgrid setup was analyzed for study of variations in parameters which are listed in Table 1. The ambiguity in the model output can be followed back to the uncertainty in the model inputs which can be depicted by sensitivity analysis. The optimization cost function is affected by the parameters and states of the model which need to be analyzed in order to study the behavior of the system in real time. The influence of different parameters on the working of microgrid setup is studied so that their effect on the model output i.e. the three-phase islanded power output. The system is studied so that it may be ranked in order of their effects and obtain initial guesses for their estimation and optimization. From the results obtained, it can be studied how robust is the cost function to incremental changes in the optimized parameters.

The parameters of the microgrid have been varied with respect to the time axis and the changes in the model output are noted which may be used for future studies. The parameters of the microgrid taken under study belongs to the active filter, battery, solar, wind and diesel generator system.

The output filter current of the microgrid setup is studied for variation by varying some parameters of the input namely coupling inductor, bypass capacitor and the controller gains. It is observed that the output filter gain is largely dependent on the bypass capacitance values. The output filter current value comes to be inversely proportional to the input capacitance values and decreases with increase in value of capacitance. The inductance values too affect the value of islanded output in lesser proportion however the value of output increases with increment in value of input. The proportional gain do not have much effect on the microgrid output This is shown in Figure 10. The statistical analysis can be seen in Figure 15.

The maximum voltage of the output and study of settling time changes have been analysed and it can be observed that the output is not influenced in a major way by any of the active filter parameters as shown in Figure 11.

The maximum voltage and settling time requirements of the three phase islanded output is studied by variations of diesel generator parameters namely the governor gain, nominal power and the rms voltage. The maximum output voltage of the microgrid is affected adversely by the change in nominal power of the diesel generator however the output increases in a positive way for changes in rms voltage value of the diesel generator which can be seen in Figure 12. The settling time is affected in the same way but at a lesser scale. The governor gain does not play a role in influencing the microgrid output. The statistics for the same can be seen in Figure 16.

Table 1. Parameters for Sensitivity Analysis

S.No	Block	Parameters	Symbols	Values
1	Active Filter	Coupling Inductor	L_a	15e-3
		Bypass Capacitor	C_b	35e-6
		Proportional Gain	K_{pa}	0.2
		Integral Gain	K_{ia}	1.5
2	Battery	Voltage	V	48
		State of Charge	SOC	98
		Response Time	t_b	10
		Proportional Gain	K_{pb}	0.1
		Integral Gain	K_{ib}	1
		FET Resistance	r_f	0.1
3	Solar PV	Irradiance	I_r	1000
		Temperature	T_s	25
4	Diesel Generator	Nominal Power	P_{nd}	24e3
		RMS Voltage	V_{rms}	110
		Frequency	f_d	50
		Governor Gain	G_d	40
5	Wind Station	Wind Speed	w_s	15
		Filter Inductance	l_w	3e-2
		Filter Capacitance	c_w	3e-4
6	Grid	Frequency	f	60
7	Other Parameters	Load Active Power	P_l	10e3
		PLL frequency	f_{pll}	60

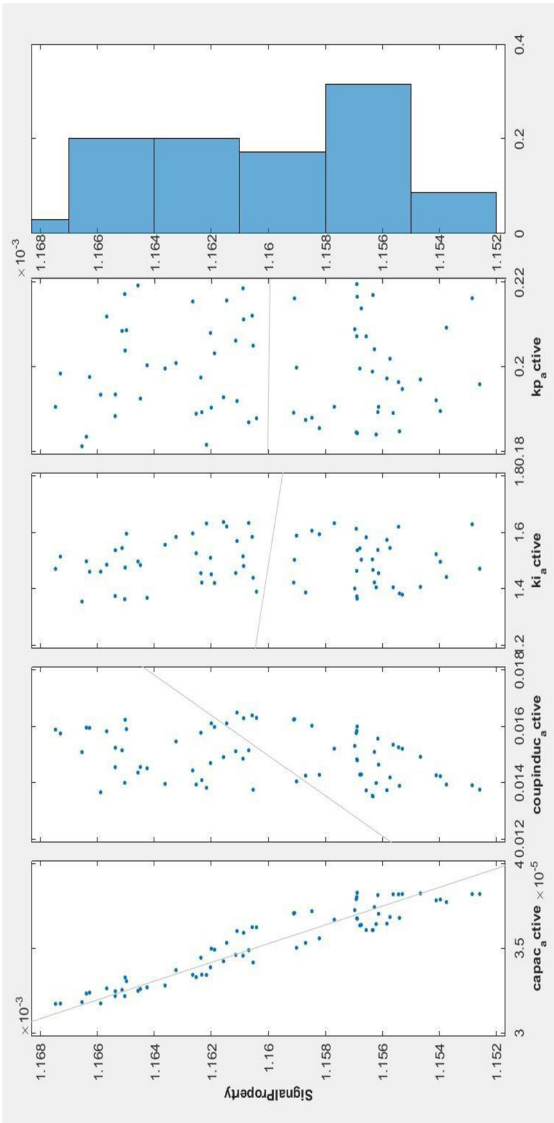

Figure 10. Variation of maximum value of filter current with variable input filter parameters

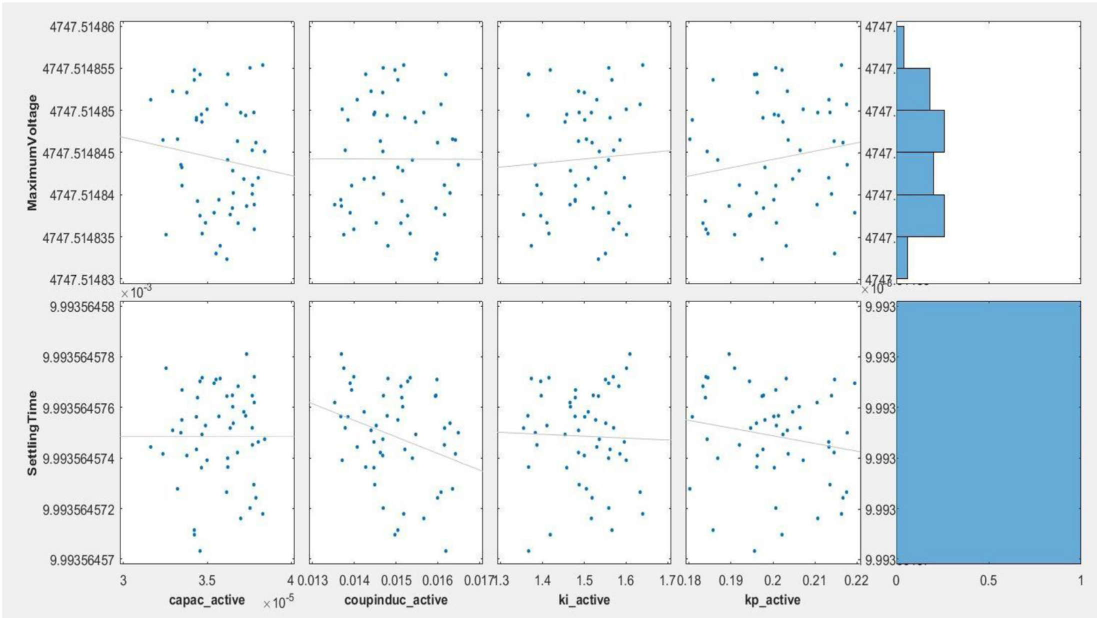

Figure 11. Variation of Maximum output voltage and settling time of microgrid with variable active filter input parameters

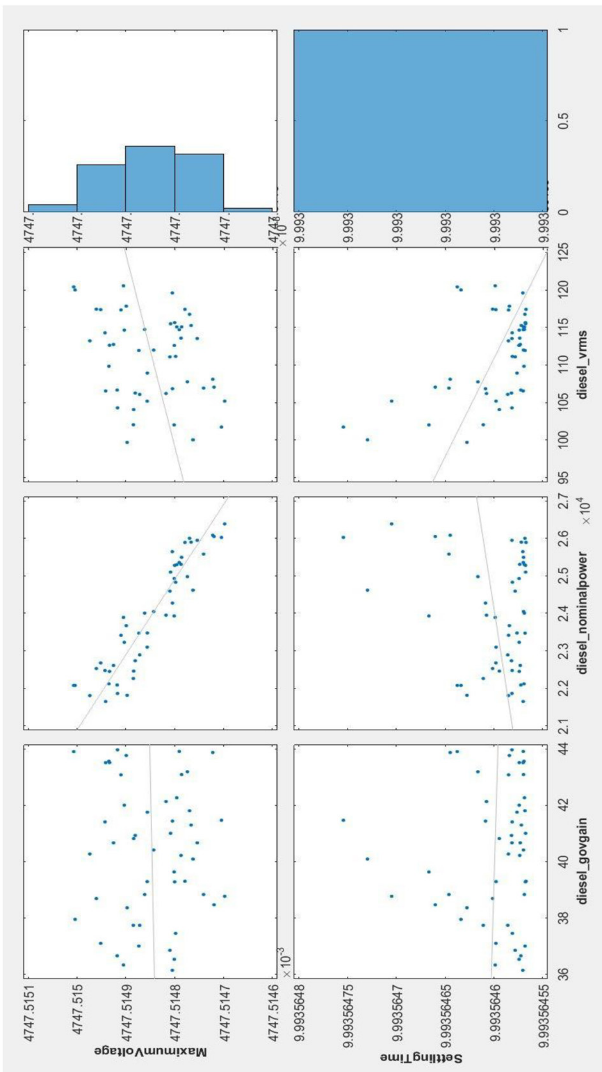

Figure 12. Variation of Maximum output voltage and settling time of microgrid with variable Diesel Generator input parameters

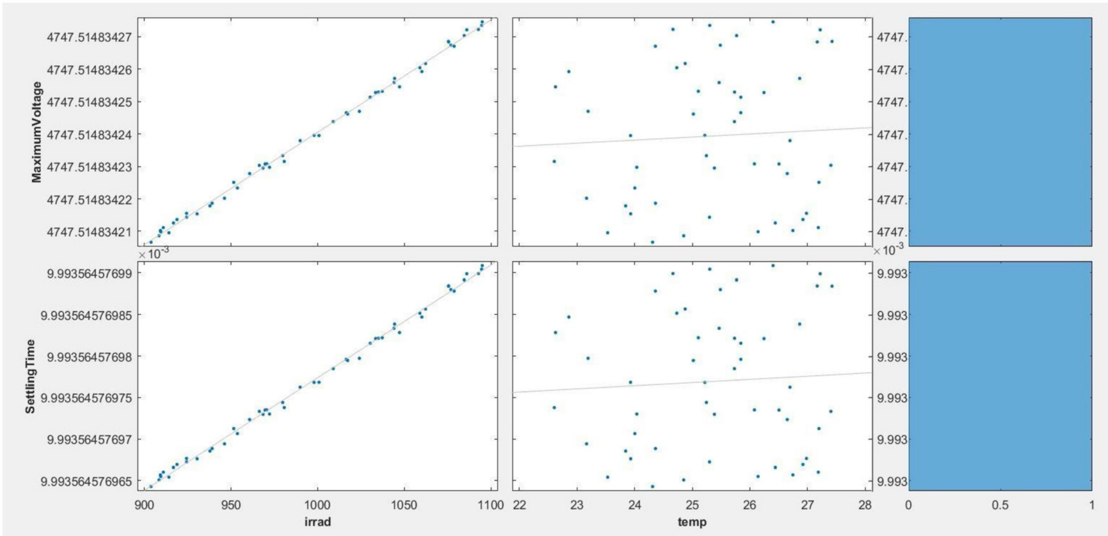

Figure 13. Variation of Maximum output voltage and settling time of microgrid with variable solar PV input parameters

The microgrid output is then studied for variations in solar parameters namely solar irradiance and surrounding temperature as shown in Figure 13. The microgrid output is affected greatly by the changes in irradiance and the output increases linearly with changes in irradiance however the temperature does not have a remarkable impact. The statistics can be seen in Figure 17.

Lastly the microgrid output is analyzed for changes in wind parameters such as wind speed and the filter inductance, capacitance as shown in Figure 14. It is observed that the filter inductance has the maximum impact on the output and the output voltage increases with increase in increase of filter inductance however the settling time decreases with increase in inductance which will not allow the system to become stable soon. The filter capacitance plays a reverse role and it is observed that the output voltage decreases with increase in filter capacitance while the settling time decreases leading to a stable output. The wind speed was not found to be influential on the model output. The statistics are plotted and shown in Figure 18.

The microgrid's total harmonic distortion (THD) of three-phase voltage has been plotted in Figure 19. The maximum harmonic distortion is found to be approximately 0.47. The results found were compared with previous similar works and shown in Table 2.

Verification and Validation of Results

From the above simulation results it is clearly observed that the suggested model has persistent DC link voltage and an entirely sinusoidal synchronized ideal voltage source. The power equilibrium between diesel generator, solar, wind, PV power system, battery and load has been preserved that validates the results achieved. It is also perceived that the suggested hybrid system behaves acceptably under diverse dynamic situations while preserving persistent voltage and frequency. To demonstrate the validity of the proposed system the percentage THD variation of output voltage waveform is assessed. One of the significant features of DG structure operation is to maintain the harmonic distortion level as minimal as possible. The harmonic level comes well within the standard limits set by IEEE, i.e., 5%.

CONCLUSION

This article proposes an active shunt filter for power quality enhancement in the islanded manner of operation. The moment at which the island event occurs can be detected including control algorithm and stabilization circuit which minimizes the harmonics of the microgrid. The mode of operation is

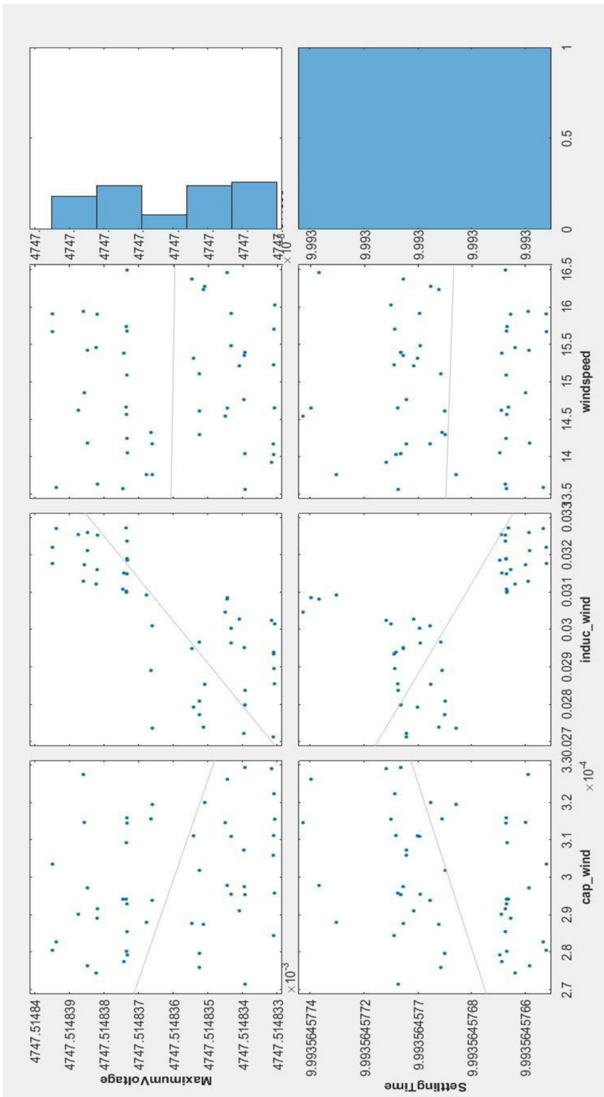

Figure 14. Variation of Maximum output voltage and settling time of microgrid with variable wind input parameters

corroborated using MATLAB software. The microgrid setup also switches from the constant-current coordinated mode to the constant voltage mode. The output of the modelled diagram is used to portray the islanding condition and its recognition and stabilization. Future studies include the study of hybrid active filters in islanded microgrids for rapid stabilization from an islanding event.

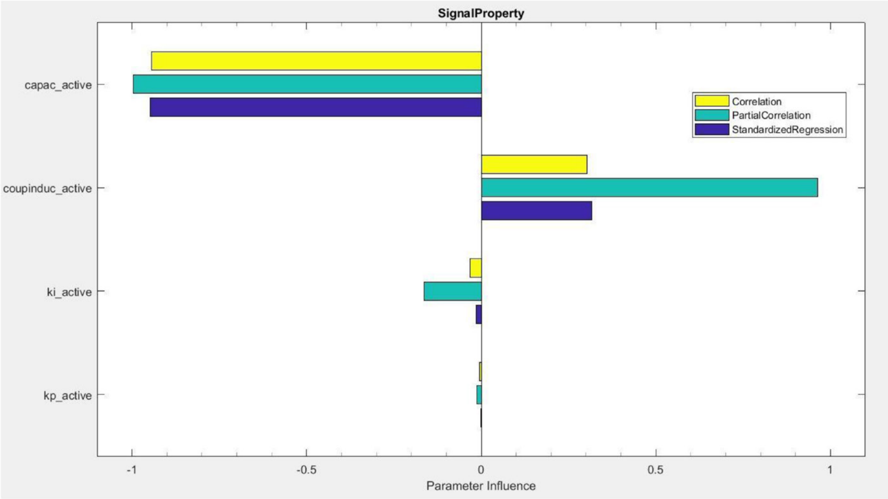

Figure 15. Statistical analysis of output filter current variation with variable input

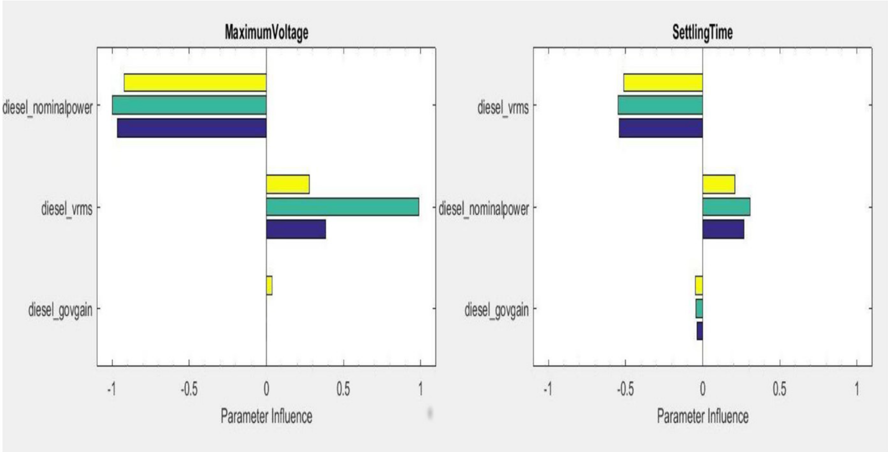

Figure 16. Statistical analysis of output filter current variation with variable input for diesel generator

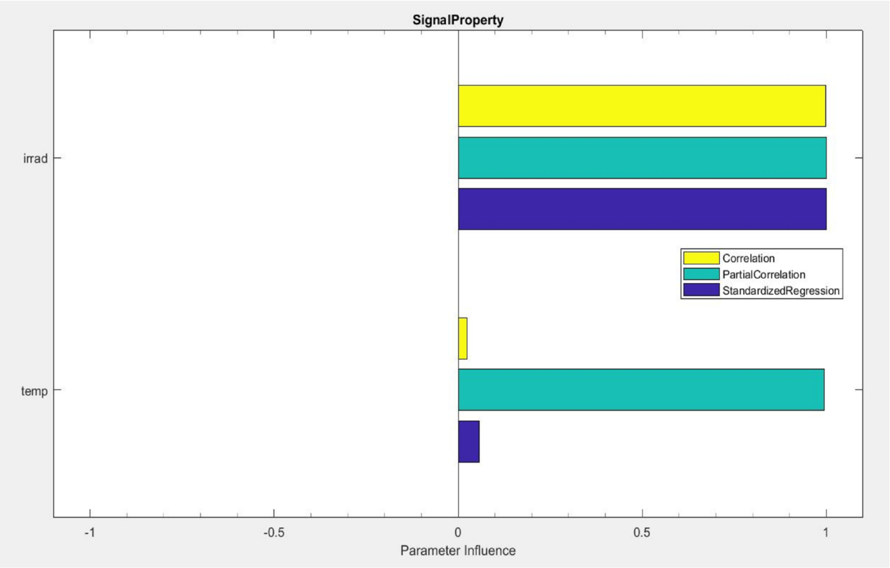

Figure 17. Statistical analysis of output filter current variation with variable solar input parameters

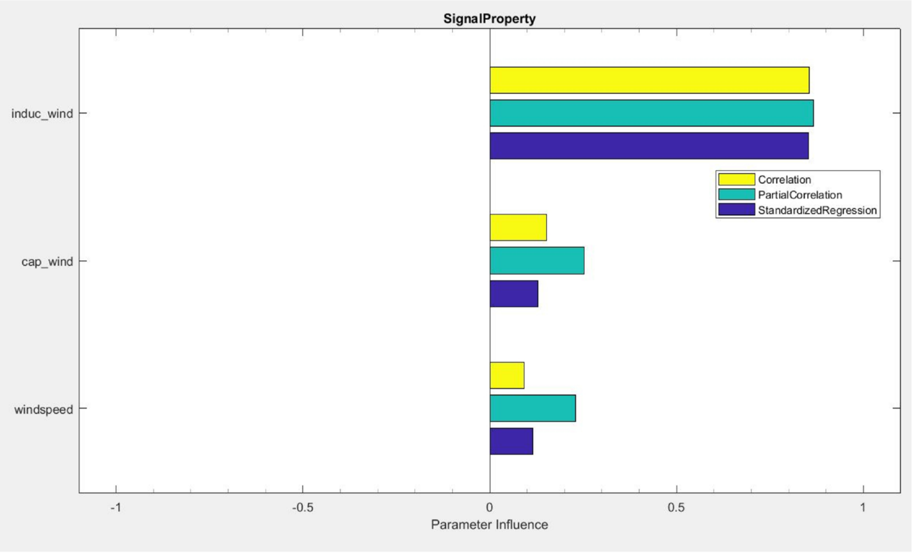

Figure 18. Statistical analysis of output filter current variation with variable wind generation inputs

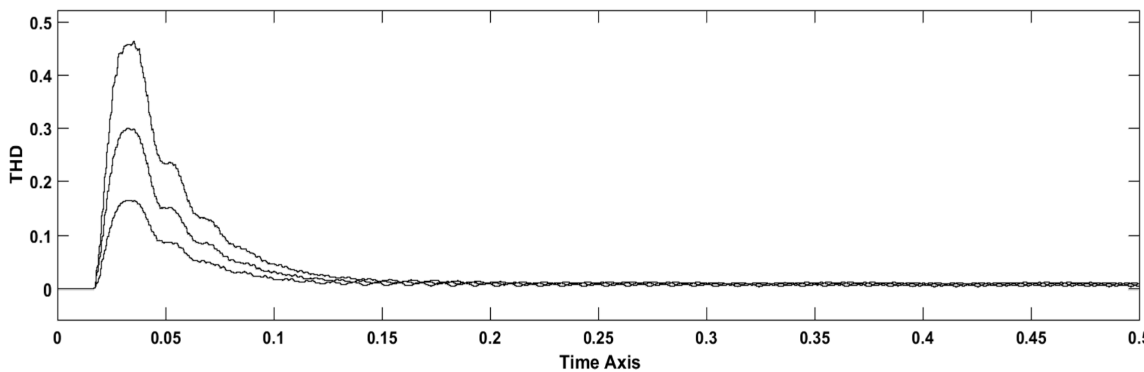

Figure 19. Total harmonic distortion of 3-phase voltage

Table 2. Comparison of prediction results with past references

References	Methods	THD_V	THD_V of proposed method
B. Nanda and R.K Jena [19]	Filter	7.82%	4.78%
Micallef et al. [20]	Capacitive virtual impedance loop	1.5%	
X. Wang et al. [10]	Inverter-interfaced Distributed Generation (DG)	3.3%	
J He et al. [21]	Adaptive hybrid voltage and current controller	4.72%	
H.M.A Antunes et al. [9]	Hybrid Filter	1.65%	

References

[1] Kuang Y, Zhang Y, Zhou B, et al. A review of renewable energy utilization in islands. Renewable and Sustainable Energy Reviews. 2016;59:504–513.

[2] Amin M. A smart self-healing grid: In pursuit of a more reliable and resilient system [in my view]. IEEE power and energy magazine. 2014;12(1):112–110.

[3] Kulmala A, Repo S, Järventausta P. Coordinated voltage control in distribution networks including several distributed energy resources. IEEE Transactions on Smart Grid. 2014; 5(4):2010–2020.

[4] Hatziargyriou N, Asano H, Iravani R, et al. Microgrids. IEEE power and energy magazine. 2007;5(4):78–94.

[5] Resende FO, Gil NJ, Lopes JP. Service restoration on distribution systems using MultiMicroGrids. European Transactions on Electrical Power. 2011;21(2):1327–1342.

[6] Demetriou P, Asprou M, Kyriakides E. A Real-Time Controlled Islanding and Restoration Scheme Based on Estimated States. IEEE Transactions on Power Systems. 2018;.

[7] Goyal M, John B, Ghosh A. Harmonic mitigation in an islanded microgrid using a DSTATCOM. Asia-Pacific Power and Energy Engineering Conference, APPEEC. 2016; 2016-Janua. Available from: 10.1109/APPEEC.2015.7380970.

[8] Srivatchan NS, Rangarajan P, Rajalakshmi S. Control Scheme for Power Quality Improvement in Islanded Microgrid Operation. Procedia Technology. 2015;21:212–215. Available from: 10.1016/j.protcy.2015.10.090.

[9] Antunes HMA, Silva SM, Brandao DI, et al. Harmonic Compensation Using a Series Hybrid Filter in a Centralized AC Microgrid. Journal of Control, Automation and Electrical Systems. 2018;29(2):219–229. Available from: 10.1007/s40313-017-0365-4.

[10] Wang X, Blaabjerg F, Chen Z. Autonomous control of inverter-interfaced distributed generation units for harmonic current filtering and resonance damping in an islanded microgrid. IEEE Transactions on Industry Applications. 2014;50(1):452–461. Available from: 10.1109/TIA.2013.2268734.

[11] Li C, Cao C, Cao Y, et al. A review of islanding detection methods for microgrid. Renewable and Sustainable Energy Reviews. 2014;35:211–220. Available from: 10.1016/j.rser. 2014.04.026.

[12] Moussa H, Martin JP, Pierfederici S, et al. Voltage harmonic distortion compensation with non-linear load power sharing in low-voltage islanded microgrid. Mathematics and Computers in Simulation. 2018;Available from: 10.1016/j.matcom.2018.05.007.

[13] Eshraghi A, Ghorbani R. Islanding detection and over voltage mitigation using controllable loads. Sustainable Energy, Grids and Networks. 2016;6(xxxx):125–135. Available from: 10.1016/j.segan.2016.02.007.

[14] Ranjbaran MEA. A power sharing scheme for voltage unbalance and harmonics compensation in an islanded microgrid. Electric Power Systems Research. 2018;155:153–163. Available from: 10.1016/j.epsr.2017.09.026.

[15] Han Y, Shen P, Zhao X, et al. An Enhanced Power Sharing Scheme for Voltage Unbalance and Harmonics Compensation in an Islanded AC Microgrid. IEEE Transactions on Energy Conversion. 2016;31(3):1037–1050. Available from: 10.1109/TEC.2016.2552497.

[16] Gui Y, Wei B, Li M, et al. Passivity-based coordinated control for islanded AC microgrid. Applied Energy. 2018;229(July):551–561. Available from: 10.1016/j.apenergy.2018.07.115.

[17] Haider R, Kim CH, Ghanbari T, et al. Harmonic-signature-based islanding detection in grid-connected distributed generation systems using Kalman filter. IET Renewable Power Generation. 2018;12(15):1813–1822.

[18] Samantaray SR, El-Arroudi K, Joós G, et al. A fuzzy rule-based approach for islanding detection in distributed generation. IEEE Transactions on Power Delivery. 2010;Available from: 10.1109/TPWRD.2010.2042625.

[19] Nanda B, Jena RK. Power Quality Analysis by using Active Filter in AC/DC Microgrid. 2018;4(9).

[20] Micallef A, Apap M, Spiteri-Staines C, et al. Reactive power sharing and voltage harmonic distortion compensation of droop controlled single phase islanded microgrids. IEEE Trans- actions on Smart Grid. 2014;5(3):1149–1158. Available from: 10.1109/TSG.2013.2291912.

[21] He J, Li YW, Blaabjerg F. Flexible microgrid power quality enhancement using adaptive hybrid voltage and current controller. IEEE Transactions on Industrial Electronics. 2014; 61(6):2784–2794.

Moving Average Filter-Pll Based Voltage and Frequency Controlof Standalone WECs

Anjana Jain[1], Saravanakumar R., and Shankar S.

ABSTRACT

Precise and fast estimation of system frequency during distorted voltage has become the main challenge for phase locked loop (PLL) for wind energy conversion systems (WECS). In this article, a moving average filter (MAF) based PLL is proposed to solve this issue for permanent magnet synchronous generator (PMSG) based WECS. A MAF allows suitable measurement of frequency and eliminates dc offset, harmonics, and unbalance in voltage. Also, the proposed scheme is able to achieve harmonics reduction. The simulation model of the underlying system is prepared in MATLAB/Simulink and its performance analysis is carried through a comparative simulation study with conventional synchronous-reference-frame (SRF) PLL, adaptive-frequency-loop PLL, type-1 PLL, and type-3 PLL. The simulation results verify that the proposed controller extracts the maximum-power from wind and stabilizes the system voltage & frequency during any variable/distorted working conditions. The simulated system performs well during dynamic and steady state condition.
Keywords: Voltage Control, Frequency Control, WECS; PMSG; BESS; VSC; PLL; MAF

INTRODUCTION

PLLs are the preferred method for integration of power and energy systems. 3-φ PLL plays an important role in frequency estimation of voltage and current during distortions and imbalance in loads or supply. Several PLLs have been proposed by the researchers [1],[16],[17]. A Newton Raphson method based harmonic-

[1]**Anjana Jain**, corresponding author anjanajain79@gmail.com. Department of Electrical and Electronics Engineering Amrita School of Engineering, Bengaluru, Amrita Vishwa Vidyapeetham, India

[2]**R. Saravanakumar**, Department of Electrical and Electronics Engineering, Amrita School of Engineering, Bengaluru, Amrita Vishwa Vidyapeetham, India, a_anjanajain@blr.amrita.edu, sarrajoom@gmail.com

Shankar S., Intel Technology India Pvt. Ltd., Bengaluru, shanks765@gmail.com

power-control is presented in [2] to tackle distorted grid and stability issues using the Lyapunov direct method. A signal processing algorithm using heterodyning moving average finite impulse response (FIR) filter with PLL removes the harmonics generated in the process from the dc signal [3]. Dual second order generalized integrator (DSOGI) PLL based on two adaptive filters excellently estimate the d-q axes components of the voltage during distorted condition with reduced computational effort [4]. Adaptive frequency loop PLL based control of voltage and frequency for PMSG based WECS is discussed in [18] and a comparative analysis of DSOGI-PLL and adaptive frequency loop PLL is presented in [19]. A robust low-pass notch filter (LPNF)-PLL is presented in [5] for grid-synchronization, which to reject the disturbances during voltage sag, imbalance, and harmonics. A straight forward discrete adaptive filter observes fundamental and harmonic sequence components of the grid voltage with improved settling time of the frequency estimation as compared to SOGI frequency locked loop (FLL) [6]. Least mean squares based algorithm features a self-learning capability to mitigate spurious tones inside the digital PLL. Adaptive least error squares (LES) filter based PLL helps in synchronization and signal decomposition [7]-[8]. A control scheme based on multi-resonator and adaptive notch filter (MRNFC) improves the frequency estimation of perturbation due to harmonics, unbalance, and faults in power systems [9]. Hybrid filtering technique including DSOGI and MAF based PLL removes fundamental frequency negative sequence (FFNS) at the pre filtering stage under distorted grid conditions.

The settling time is less than one cycle [10]. The fourth order generalized integrator (FOGI) using is utilized to draw maximum power from solar PV with improved power quality with harmonic rejection capability [11]. A differentiation PLL spots unbalance in phase and enhances the performance during transients by reducing the settling time and mean square error [12]. A control scheme based on MAF is applied for 1-φ system. Scheme uses a multiplier as phase detector for a distorted grid voltage to avoid detection error. A predictive rule compensates the delay caused by MAF [13]. The general description and main challenge associated with MAFs with their solutions are discussed by the author along with their capabilities and limitations for different types of application based MAF-PLLs. PID-type loop filter (LF) can provide a higher bandwidth with speedy transient response in comparison to PI- LF, but noise immunity and disturbance-rejection capability will reduce [14].

This article is organized as follows: The introduction and literature survey are presented first. Then, the system description and control scheme is given. Next, simulation results and discussion are presented. Finally, a conclusion is stated.

SYSTEM DESCRIPTION & CONTROL SCHEME

Voltage & frequency are not constant for variable speed WECS. Variations in the voltage & frequency can be controlled with a proper controller and a satisfactory operation during any load or wind velocity variation can be achieved. Figure 1 presents the system configuration. It is comprises of Wind-turbine (WT), PMSG, 3-φ variable load (linear/non-linear), voltage source converter (VSC), Battery Energy Storage System (BESS). A WT is connected to PMSG [15] and PMSG is supplying the variable load. The non-linear load is a combination of rectifier and R-L components. BESS along with PMSG supplies the load during low wind-velocity and battery stores excess power supplied by PMSG during high wind-speed. MAF-PLL controller is utilized during variable wind-velocities, variable load, load unbalancing, and faults. Figure 2 (a,b&c) shows the conventional SRF-PLL, adaptive-frequency-loop PLL, and MAF-PLL based controls.

MAF-PLL based controller

MAF is a linear phase low pass filter and. The open loop bandwidth is reduced by addition of a MAF into PLL. Due to increasing integration of renewable-energy-sources to the and due to nonlinear/unbalanced distorted loads, synchronization has become difficult and challenging. Then PLL with enhanced disturbance rejection capability are required with extra filters. For MAF:

$$y(t) = \frac{1}{T_\omega} \int_{t-T_\omega}^{t} x(\tau)\, d\tau \tag{1}$$

Where, is the input signal and is the output signal for MAF. is the is the MAF window length. The MAF passes the dc component and completely blocks frequency components of integer multiples of . In Laplace domain, transfer function for MAF is:

$$\mathrm{MAF}(s) = \frac{1-e^{-sT_\omega}}{sT_\omega} \tag{2}$$

MAF completely stops frequencies of integer multiples of and allows only dc components. Slower transient response and delay in phase will appear when the MAF's window width . Other choices of window width are & , suitable in presence of odd-order harmonics in the input of PLL. A properly selected value of window width can block all the characteristic harmonics. Where, is defined as the nominal period of the input signals of MAF-PLL.

To regulate the terminal voltage & frequency is the main objective of the converter. For standalone WECS grid is absent, terminal voltage is to be controlled with respect to its magnitude and its frequency. So the control scheme for standalone WECS consists of frequency loop controller and voltage loop controller. References for load-current are generated using MAF-PLL and PI controllers. MAF-PLL is utilized for estimation of system frequency. d-q axis load current references are found from voltage and frequency loop and transformed to three abc component with the help of inverse-Park's-transformation (ILabc*). Then control pulses are generated and fed to a bi-directions voltage source converter (VSC).

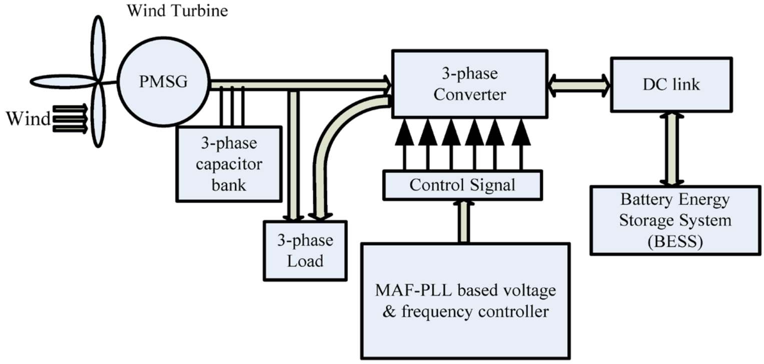

Figure 1. System configuration

Estimation of d-axis reference current

The frequency error $f_e(n)$, the difference of measured & reference frequencies, is given to PI controller. d-axis reference is found from PI controller's output and the weighted average amplitude of the d-axis load current.

$$f_e(n) = f_{rf}(n) - f(n) \tag{3}$$

$$I_d^*(n) = I_d(n-1) + k_{pd}\{f_e(n) - f_e(n-1)\} + k_{id} f(n) \tag{4}$$

$f_{rf}(n)$ = reference frequency, $f(n)$ = measured frequency of the system, k_{pd} & k_{id} = constant of PI controller in the frequency loop.

Estimation of q-axis Reference Current

The terminal voltage error $V_{te}(n)$, the difference between measured & reference voltages, is given to PI controller. q-axis reference current is found from PI controller's output and the weighted average amplitude of the q-axis load current.

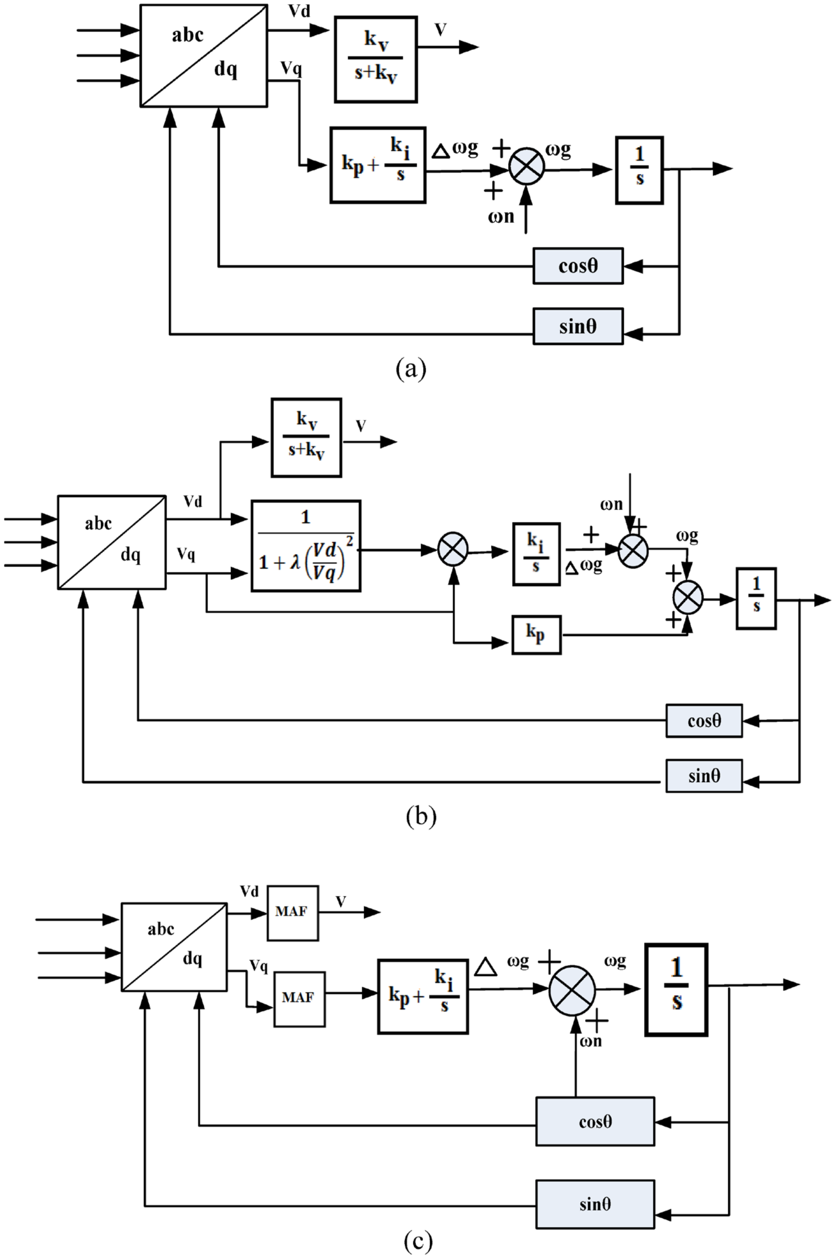

Figure 2. Schematic diagrams of (a) conventional SRF PLL, (b) adaptive-frequency-loop PLL, and (c) MAF-PLL [1]

$$V_{te}(n) = V_{trf}(n) - V_t(n) \tag{5}$$

$$I_q^*(n) = I_q(n-1) + k_{pq}\{V_t(n) - V_t(n-1)\} + k_{iq}V_t(n) \tag{6}$$

V_{trf} (n) = reference terminal voltage, V_t (n) = measured terminal voltage, k_{pq} & k_{iq} are constants of PI controller in voltage loop.

SIMULATION RESULTS AND DISCUSSION

Simulation analysis of the proposed system is done to see performance and effectiveness of the WECS for variable working conditions.

Effect of Variations in Wind-Velocity During Constant Load

A constant 3-φ balanced load of 5kW, which is coupled at PCC of the system. System started with a wind velocity of 12m/s. At t = 0.25s, wind velocity is 10m/s, and changed to 13m/s at t = 0.55s. Figure 3(a) shows that voltage & frequency are steady regardless of any change in the wind velocity. PMSG generated power is proportional to wind velocity. Battery gets charge when PMSG generates excess power due to super synchronous speed and get discharge when PMSG generates lesser power due to sub synchronous speed.

Effect of Variations in Load During Constant Wind-Velocity

System is running with a wind velocity of 13m/s with a constant load of 5kW. At t = 0.7s load is changed to 6kW by adding another load of 1kW and load is made unbalanced during t = 0.85s to 1.0s. It can be viewed from the Figure 3(a) that the voltage & system frequency are steady regardless of any disturbance in the load. Charging or discharging of BESS takes place via VSC to absorb the variations in the load and provide power balancing. Thus load can be supplied at a steady voltage & frequency. Wind velocity, rotor speed, system-frequency, terminal voltage, and generator's, load's, converter's currents are shown in Figure 3(a). 3-φ waveforms of terminal voltage, generator current, load current, converter current are shown in Figure 3(b). Active & reactive powers of generator, load, and converter are presented in Figure 3(c). It can be concluded that system works effectively under different operating conditions. Table 1 gives the details about the system performance.

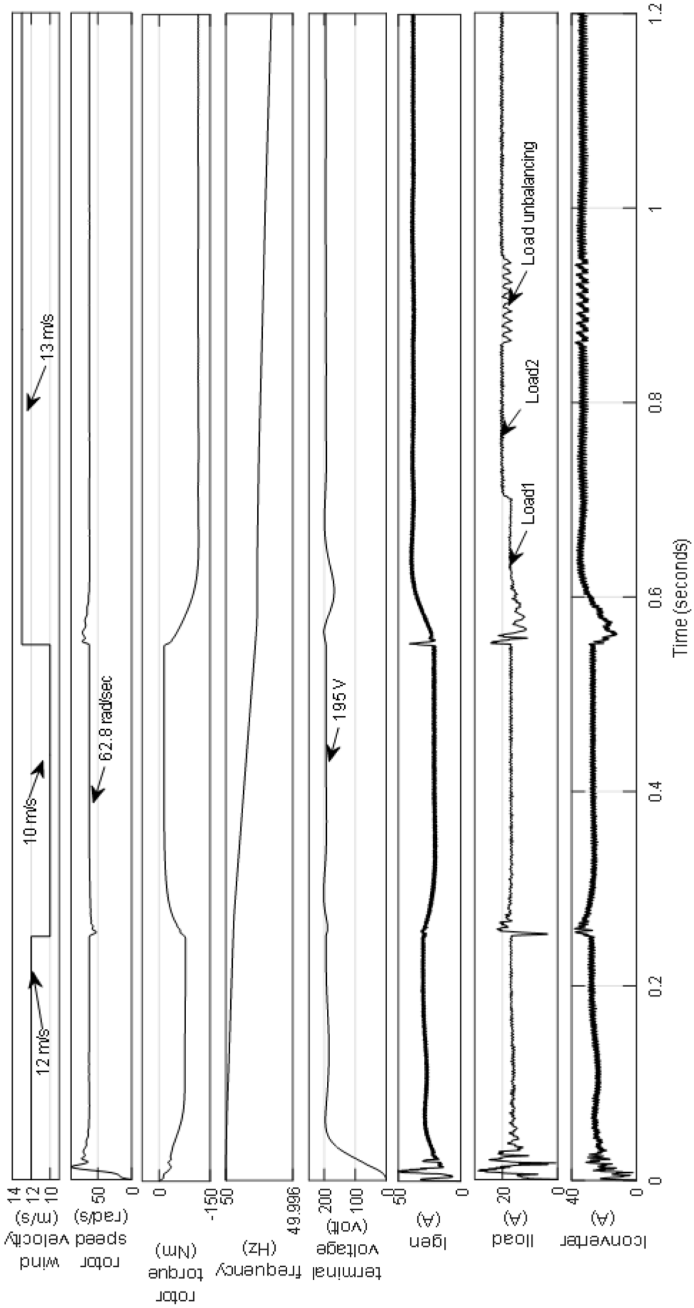

(a)

Figure 3.
(a, b, c) performance of WECS under variable wind velocity & load

(Continued)

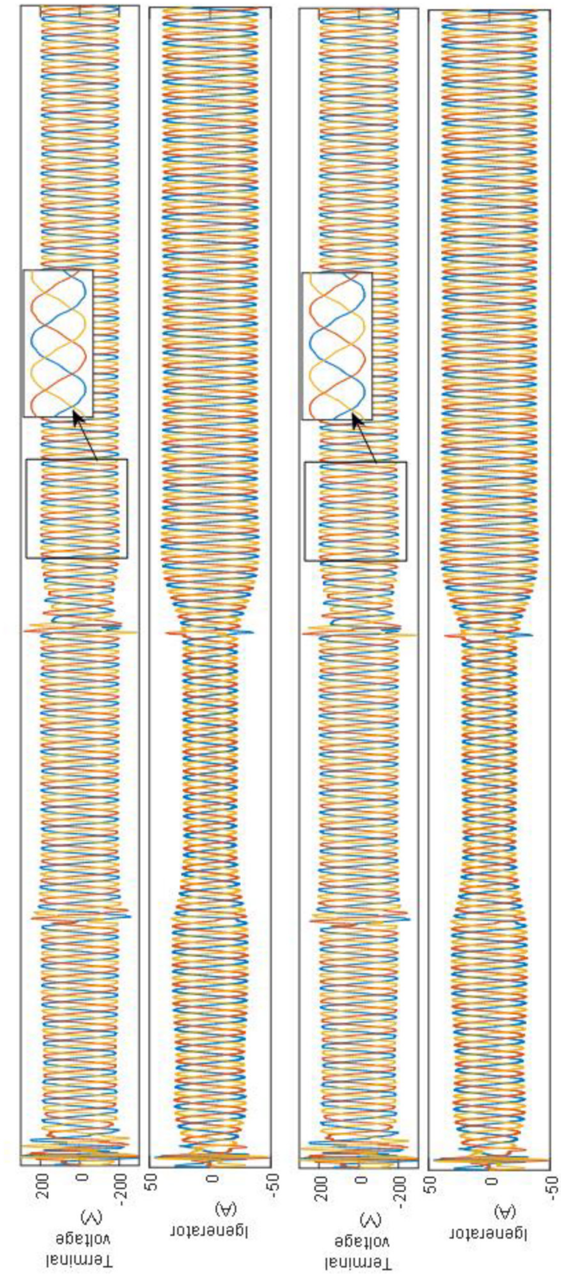

(b)

Figure 3.
(a, b, c) performance of WECS under variable wind velocity & load

(Continued)

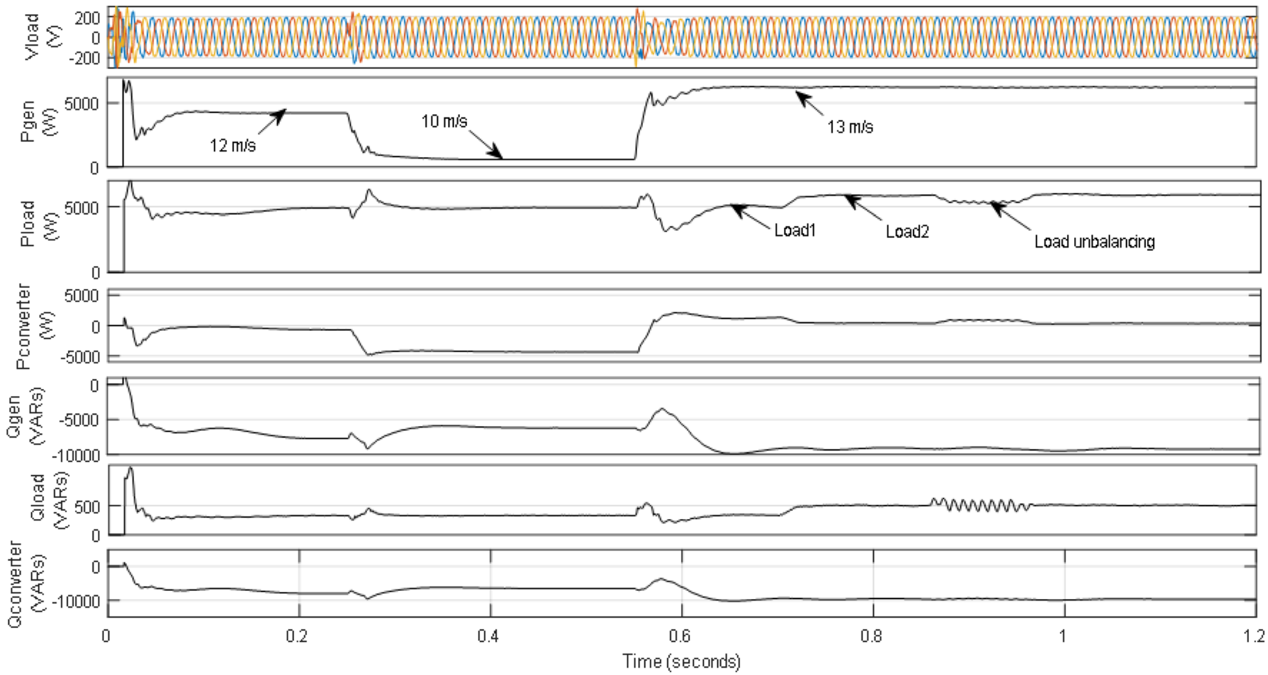

(c)

Figure 3.
(a, b, c) performance of WECS under variable wind velocity & load

(*Concluded*)

Table 1. System performance during varying working conditions

Here, $P_{Gen} - P_{Load} = P_{Converter}$, $Q_{Gen} - Q_{Load} = Q_{Converter}$, is verified.

Particulars	wind-velocity			load			
				Load 1	Load 2	Load unbalancing	Load balancing
Wind velocity v (m/s)	12	10	13	13	13	13	13
Frequency F(Hz) approx.	50	50	50	50	50	50	50
Terminal voltage peak V_t (V)	195	195	195	195	195	195	195
Generator active power P_{Gen} (W)	4190	570	6220	6220	6220	6220	6220
Load active power P_{Load} (W)	4920	4920	4920	4920	5920	5400	5920
Converter active power $P_{Converter}$ (W)	-730	-4350	1300	1300	300	820	300
Generator reactive power Q_{Gen} (VAR)	-773(	-6200	-9180	-9180	-9180	-9180	-9180
Load reactive power Q_{Load} (VAR)	330	330	330	330	510	510	510
Converter reactive power $Q_{Converter}$(VAR)	-806(	-6530	-9510	-9510	-9690	-9690	-9690

Effect of L-G fault

The controller's operation during L-G fault is analyzed under constant wind velocity of 13m/s with a constant 3-φ balanced load of 6kW coupled at PCC of the system. System started with the wind-velocity of 13m/s. An L-G fault is created during t = 0.3sec to t = 0.35sec. It is observed that the system frequency is maintained constant at 50Hz and the voltage at PCC is getting affected. The current is raised with significant decrease in the voltage for the corresponding phase. Wind velocity, terminal voltage, 3-φ voltage at PCC, generator current, load current, converter current, generator power, load power, and converter power are presented in Figure 4 (a&b). The variations in the load current and power are being absorbed by BESS for load balancing.

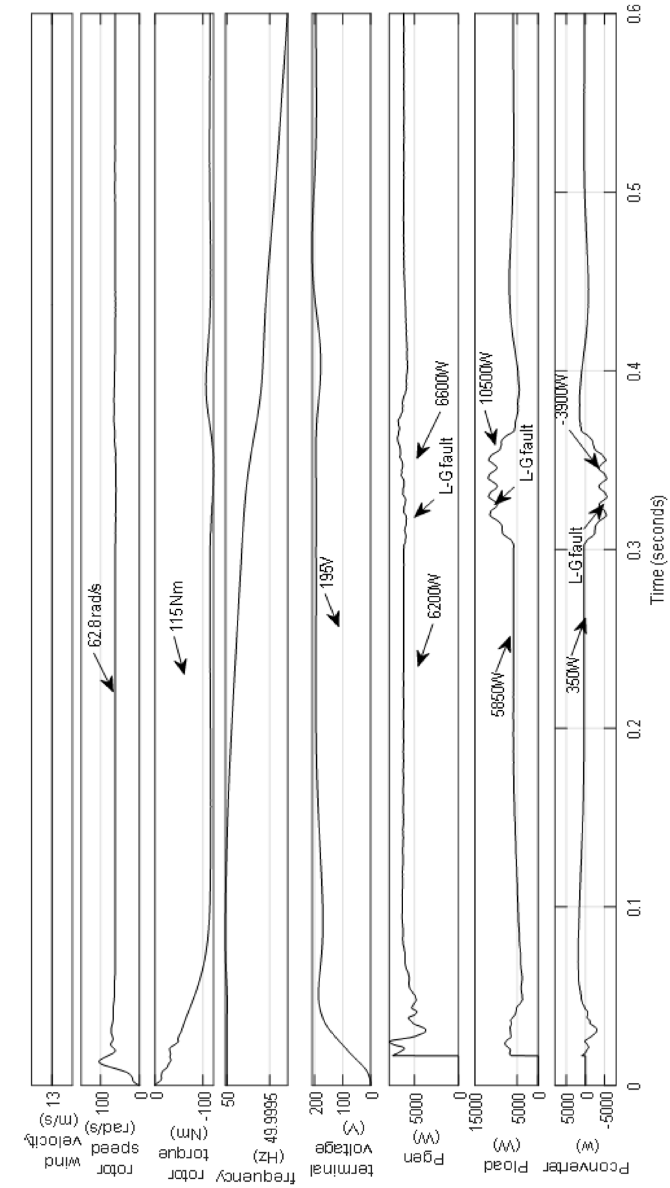

(a)

Figure 4. (a&b) performance of WECS under L-G fault

(Continued)

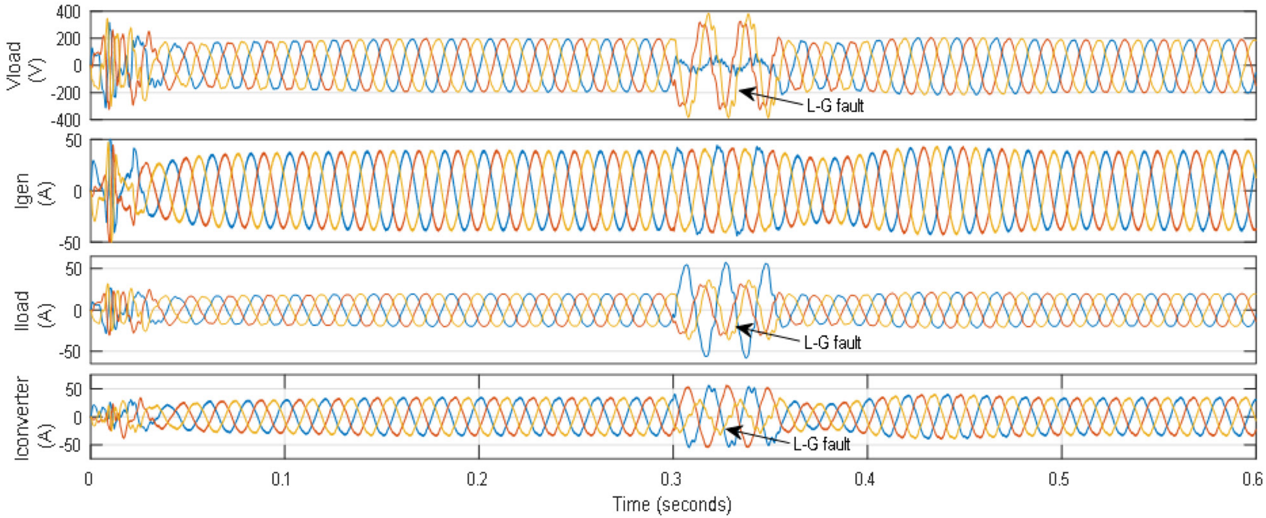

(b)

Figure 4. (a&b) **performance of WECS under L-G fault**

(Concluded)

THD (Total Harmonic Distortion) Analysis of the System

THD analysis is carried out and presented in Figure 5(a,b,c). It is observed that %THD is under the allowable limits. Table 2 shows the %THD for load voltage & current, and source currents and Table 3 gives the percentage of different orders of harmonics present in the generator voltage for different PLL based schemes. Time response analysis of terminal voltage for different PLL schemes under varying wind velocity is carried out and presented in Figure 6. MAF shows comparatively satisfactory response.

CONCLUSION

In this article, a controller based on MAF-PLL for PMSG-BESS based standalone WECS is proposed. Proposed controller is able to keep steady terminal voltage & frequency during varying working environment: like variable wind velocity and variable load (linear/nonlinear load and unbalanced load). The controller work satisfactorily in all these situations and reduce the harmonics during load or wind-velocity disturbances. BESS assisted PMSG based WECS provides load power balancing. The analysis in MATLAB/Simulink environment verifies the controller's performance and effectiveness through its fast dynamic response. THD analysis for source (generator) voltage, source (generator) current, and load current is found as 3.22%, 2.31%, and 4.69% respectively, which are within the allowable limits. The THD analysis for conventional SRF-PLL, adaptive frequency loop-PLL, type-1 PLL, and type-3 PLL is carried out and the results are presented in the above sections. It is found that MAF shows better response than other PLLs discussed under comparison.

References

[1] Saeed Golestan, Josep M. Guerrero, AND Juan C. Vasquez (2017). Three-Phase PLLs: A Review of Recent Advances. IEEE Transaction on Power Electronics, vol. 32(3), pages 1894-1907.

[2] Min Dai, Mohammad Nanda Marwali, Jin-Woo Jung, and Ali Keyhani (2008). Power Flow Control of a Single Distributed Generation Unit. IEEE Transaction on Power Electronics, vol. 23(1), pages 343-352.

[3] Francisco D. Freijedo, Jesus Doval-Gandoy, Oscar Lopez, Pablo Fernandez-Comesana, and Carlos Martinez-Penalver (2009). A Signal-Processing Adaptive Algorithm for Selective Current Harmonic Cancellation in Active Power Filters. IEEE Transaction on Industrial Eelectronics, vol. 56(8), pages 2829-2840.

[4] Pedro Rodrıguez, Alvaro Luna, Raul Santiago Munoz-Aguilar, Ion Etxeberria-Otadui, Remus Teodorescu, and Frede Blaabjerg (2012). A Stationary Reference Frame Grid Synchronization System for Three-Phase Grid-Connected Power Converters Under Adverse Grid Condition. IEEE Transaction on Power Electronics, vol. 27(1), pages 99-112.

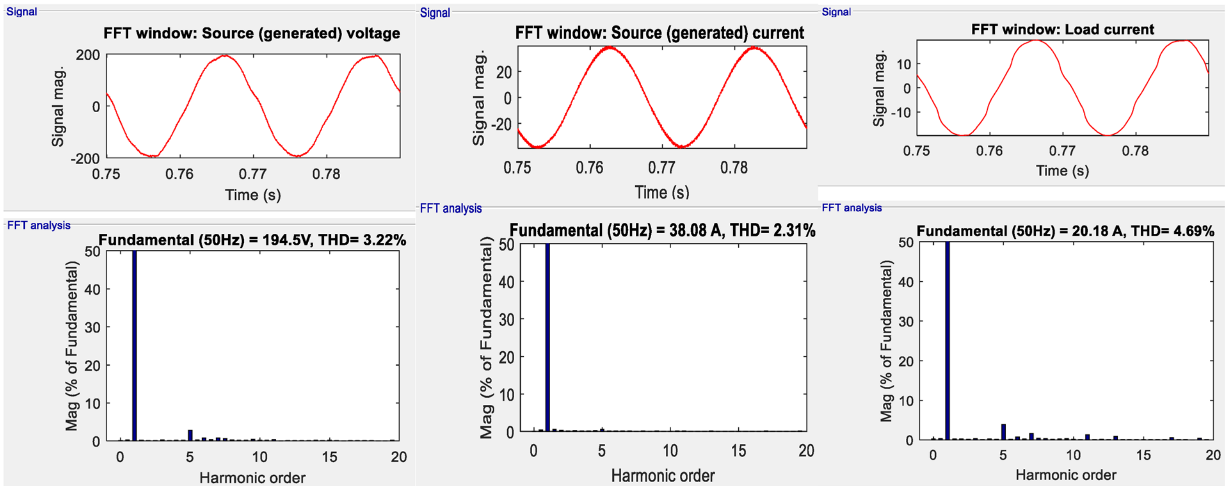

(a) (b) (c)

Figure 5. Waveform and % THD (a) source (generator) voltage, (b)source (generator) phase-current, and (c) load current

Table 2. % THD analysis

Parameters → / Type of PLL ↓	Source (generator) voltage	Source (generator) current	Load current
MAF-PLL	3.22	2.31	4.69
Adaptive frequency loop-PLL	4.28	2.39	5.27
Conventional SRF-PLL	3.26	2.35	4.22
Type-1 PLL	4.24	4.4	4.36
Type-3 PLL	11.48	3.94	10.04

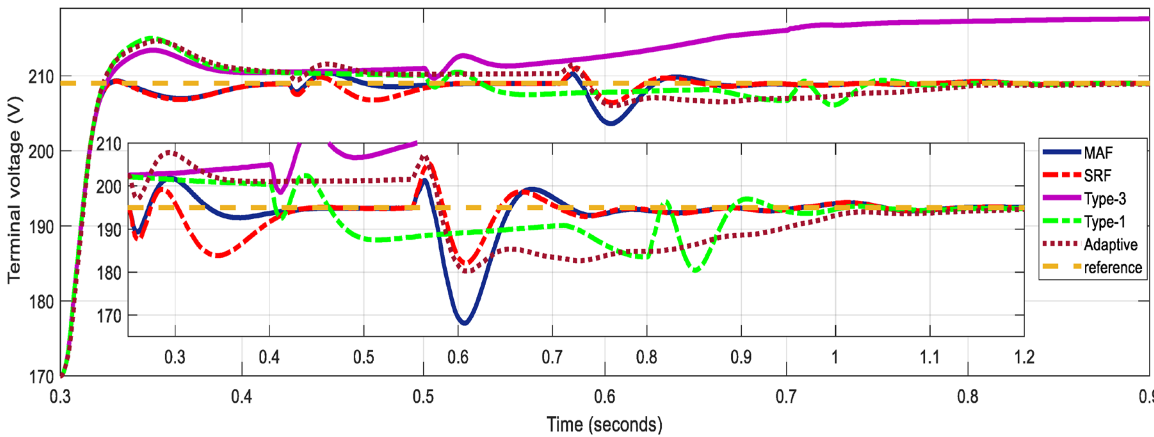

Figure 6. Time response of terminal voltage with different PLLs

Table 3. % THD analysis of generator (source) voltage

Order of harmonics	MAF-PLL	Adaptive frequency loop PLL	Conventional SRF-PLL	Type-1 PLL	Type-3 PLL
1st	193V, 100%	182V, 93.33%	195V, 100%	188.9V, 96.87%	224.7V, 18.23%
2nd	1.21V, 0.62%	0.05V, 0.025%	1.91V, 0.98%	2.44V, 1.25%	2.4V, 1.23%
3rd	0.85V, 0.44%	0.57V, 0.29%	0.21V, 0.11%	1.11V, 0.57%	1.65V, 0.85%
4th	0.64V, 0.33%	0.56, 0.29%	0.43V, 0.22%	0.41V, 0.21%	3.26V, 1.67%
5th	5.34V, 2.74%	2.87V, 1.47%	5.02V, 2.57%	3.26V, 1.67%	22.69V, 11.64%
6th	1.33V, 0.68%	0.54V, 0.28%	0.9V, 0.46%	0.5V, 0.26%	1.75V, 0.90%
7th	3.04V, 1.56%	6.72V, 3.44%	1.67V, 0.86%	6.1V, 3.13%	9.89V, 5.07%
% THD	3.22%	4.28%	3.26%	4.24%	11.48%

[5] Kyoung-Jun Lee, Jong-Pil Lee, Dongsul Shin, Dong-Wook Yoo, and Hee-Je Kim (2014). A Novel Grid Synchronization PLL Method Based on Adaptive Low-Pass Notch Filter for Grid-Connected PCS. IEEE Transaction on Industrial Electronics, vol. 61(1), pages 292-301.
[6] Xiangjun Quan, Xiaobo Dou, Zaijun Wu, Minqiang Hu, and Feng Chen (2017). A Concise Discrete Adaptive Filter for Frequency Estimation Under Distorted Three-Phase Voltage. IEEE Transaction on Power Electronics, vol. 32(12), pages 9400-9412.
[7] Rotem Avivi, Michael Kerner, Evgeny Shumaker, Giuseppe Li Puma, Tami Sela, Lidor Sofer, and Gil Horovitz (2017). Adaptive Spur Cancellation Technique in All-Digital Phase-Locked Loops. IEEE Transaction on Circuits and Systems II: Express Briefs, vol. 64(11), pages 1292-1296.
[8] Saeed Golestan, Esmaeil Ebrahimzadeh, Josep M. Guerrero, Juan C. Vasquez, and Frede Blaabjerg (2017). An Adaptive Least-Error Squares Filter-Based Phase-Locked Loop for Synchronization and Signal Decomposition Purposes. IEEE Transaction on Industrial Electronics, vol. 64(1), pages 336-346.
[9] Zahra Dehghani Arani, Seyed Abbas Taher, Amir Ghasemi, and Mohammad Shahidehpour (2019). Application of Multi-Resonator Notch Frequency Control for Tracking the Frequency in Low Inertia Microgrids under Distorted Grid Conditions. IEEE Transactions on Smart Grid, vol. 10(1), pages 337-349.

[10] Yunlu Li, Junyou Yang, HaixinWang, Weichun Ge, and Yiming Ma (2018), A Hybrid Filtering Technique-Based PLL Targeting Fast and Robust Tracking Performance under Distorted Grid Conditions. Energies-Open Access Journal of Energy Research, Engineering and Policy, vol. 11(4), pages 1-18.

[11] Priyank Shah, Ikhlaq Hussain, and Bhim Singh (2018). A Novel Fourth Order Generalized Integrator Based Control Scheme for Multifunctional SECS in the Distribution System. IEEE Transaction on Energy Conversion, vol. 33(3), pages 949-958.

[12] Sanchit Mishra, Ikhlaq Hussain, Geeta Pathak, and Bhim Singh (2018). dPLL-based control of a hybrid wind–solar grid connected inverter in the distribution system. IET Power Electronics, vol. 11(5), pages 952-960.

[13] Menxi Xie1,CanYan Zhu, BingWei Shi, and Yong Yang (2017). Power Based Phase-Locked Loop Under Adverse Conditions with Moving Average Filter for Single-Phase System. Journal of Electrical Systems, vol. 13(2), pages 332-347.

[14] Saeed Golestan, Malek Ramezani, Josep M. Guerrero, Francisco D. Freijedo, and Mohammad Monfared (2014). Moving Average Filter Based Phase-Locked Loops: Performance Analysis and Design Guidelines. IEEE Transaction on Power Electronics, vol. 29(6), pages 2750-2763.

[15] Ashish Patel, Sabha Raj Arya, Anjana Jain (2016). Variable step Learning Based Control Algorithm for Power Quality in PMSG Based Power Generation System. 2016 IEEE 7th Power India International Conference (PIICON), India.

[16] Anjana Jain, S. Shankar, Vanitha V. (2018). Power Generation Using Permanent Magnet Synchronous Generator (PMSG) Based Variable Speed Wind Energy Conversion System (WECS): An Overview. Journal of Green Engineering, vol. 7(4), pages 477–504.

[17] Anjana Jain, Shashwat Trivedi, Paras Sharma, Shyam Gopal Reddy, R. Chaitanya, and S. Shankar (2018). Simulation study of Permanent Magnet Synchronous Generator (PMSG) connected to variable speed Wind Energy Conversion System (WECS). 2017 International Conference on Trends in Electronics and Informatics (ICEI), India.

[18] Anjana Jain, R. Saravanakumar, S. Shankar, V. Vanitha (2018). Adaptive SRF-PLL Based Voltage and Frequency Control of Hybrid Standalone WECS with PMSG-BESS. International Journal of Emerging Electric Power Systems, vol. 19(6).

[19] Anjana Jain, R. Saravanakumar (2019). Comparative Analysis of DSOGI-PLL & Adaptive Frequency Loop-PLL for Voltage and Frequency control of PMSG-BESS based Hybrid Standalone WECS. 8th International Conference on Power and Energy Systems, Sri Lanka.

Simple Approach to Estimating PV System Snow Losses Applied to Long-term PV Generation Datasets for Different Tilt Angles and Mounting Styles

Erik Janssen, David Nixon, Svend De Bruyn, Gil Amdurski and Leigh St. Hilaire
Sustainable Technologies Evaluation Program (STEP) of Toronto and Region Conservation Authority (TRCA), Vaughan, ON, L4K 5R6, Canada

ABSTRACT

In a cold climate, it's important to evaluate the snow coverage of photovoltaic (PV) arrays. General snow loss models and values are available in the literature, but the actual snow losses are specific to local climate conditions. Thus, most generic models have not been validated for specific locations. This study presents measured power yield and estimated snow loss data spanning from 2011 to 2017 from PV arrays located in Ontario, Canada, mounted at several different tilt angles, also considering pole and roof-mounting styles. The data is itself useful for snow loss model validation, and the approach used to estimate snow losses is simple and easily applied to other installations. It only requires daily energy generation data that is commonly available to system owners, which is then used in conjunction with free software tools and environmental datasets available online. This proposed approach allows systems owners to estimate snow losses more directly based on their own system energy generation data. Empirical data on snow losses is useful to system owners for a variety of reasons. For example, it can quantify the lost revenue, inform decision-making around snow removal, help explain shortfalls and variations in energy yield, and provide useful information for buildings seeking net-zero energy. Also, the approach can be used to more accurately evaluate the techno-economic feasibility of a prospect PV project for a given snowy region, provided the model has been previously validated for such a region.

INTRODUCTION

Modelling tools for photovoltaic (PV) installations are capable of highly accurate results. However, in a cold climate, modules will sometimes be entirely covered by snow and this is difficult to predict within a model. A recent report from the National Renewable Energy Laboratory (NREL) [1] summarized that there have been a range of different snow loss values reported in the literature and various efforts to generate snow loss models (as an example, see [2]). A significant issue is that models have not been widely validated and losses vary with local climates. In general, the modeling community is still in need of a widely validated solution. The researchers from [1] propose the model from [3], now integrated into NREL's System Advisor Model (SAM) modeling tool. They showed that the model generated better agreement with actual generation data for two installations. However, they note that the model is best at estimating annual losses and worse agreement is seen at shorter timescales, suggesting that there is still significant room for improvement.

In the literature, the different approaches to estimating PV system snow losses might be placed in two categories. The first category, used in [1], is to show that the application of a snow loss model generates better agreement with actual PV system energy generation. The actual losses due to snow could then be determined by modeling the system both with and without the snow loss component of the model. However, for a model to achieve good agreement at all, regardless of snow, all model parameters need to be accurately defined. This could be done through an iterative calibration process where certain model parameters are adjusted until good agreement is achieved. This may be an onerous process that is not feasible for many system owners that could benefit from snow loss estimates.

The second category is to devise an experimental set-up that more directly determines the losses without explicitly needing a model to estimate them. This can involve thermostatically-heated modules (that would never by covered in snow) compared to non-heated modules [4-5], direct removal of snow from one module in a matched pair [6], or additional on-site irradiance measurements [7]. The drawback of the first category is that it is not necessarily as robust as more direct experimental measurements, and the calibration of the model can be potentially onerous. The drawback of the second category is that the set-up used to experimentally determine losses can itself be onerous—requiring measurements or other equipment not typically available in general installations.

This article provides long-term snow loss data from a set of installation in Toronto, ON, Canada, and outlines a more straightforward approach to estimating snow losses that relies only the typically available data for most PV installations. As will be shown, the approach used in this study did incorporate PV system modeling but it was simple and only required a few input parameters. In fact, the only requirement on the PV system model was that it was sufficient to catch outlier data, and then quantify the extent to which that data was an outlier. This meant that the model parameters could be much more loosely defined, and no significant model calibration process was required. It is therefore more accessible to a broader segment of PV system owners that can benefit from snow loss estimates for their installations.

STUDY SITE

In 2010, a number of PV arrays were installed at the Sustainable Technologies Evaluation Program (STEP) PV Test Lab located near Toronto, ON, Canada, to investigate snow losses. Different mounting styles were considered. Pairs of modules were ground-mounted on poles in portrait orientation at tilt angles of 0°, 10°, 20°, 30°, 40°, 70° and 90° (Figure 1). The module pair mounted at 40° was an exception—one module was mounted in portrait orientation and the other, in landscape. An array of eight modules was installed on a roof-section with a roof slope of 30° (Figure 2). Four were mounted in portrait orientation and four in landscape. An array of four modules mounted with ballast on a flat deck (Figure 3).

Pole-mounted modules were from Sanyo (HIP-190BA2) with a maximum power point of 190W. These modules were removed from a previous installation and were manufactured in 2003. As of 2019 there was notable delamination along the busbars of the PV cells—this would affect the specific yield but not the estimates of snow losses. Modules on the roof-section and on the flat deck were from Solgate (SG17524) with a max power point of 175 W. They were manufactured in 2010. As of 2019, no notable issues were apparent from visual inspections. The Inverters were M200 or M190 Series from Enphase. The azimuthal orientation of the modules was due South and there were no shading objects. Modules were not actively cleaned. Module-level daily energy data from 2011 to 2017 was obtained from the Enphase Enlighten monitoring portal. In this study, loss estimates hinged on a comparison of actual and modeled energy. SAM was used for modeling, and environmental data was obtained from NREL's National Solar Resource Database (NSRDB).

ANALYSIS

Modelled energy data was compared to actual energy data for each day of the study period from 2011 to 2017 and for each module. The modeling was used to identify days affected by snow coverage and estimate the energy that was lost. The approach used to estimate snow losses is summarized below.

Figure 1.
Several modules pairs were mounted on poles at different tilt angles

Figure 2. Eight modules were mounted on a roof-section.

Figure 3. Four modules were mounted with ballast on a flat deck.

1) *Compile daily actual energy generation data from the installation and download environmental data* for the site from the SRDB covering the same span of time as the actual data.

2) *Create a simple model of the system in SAM*. The model inputs are array tilt, azimuth, inverter and module models. Losses were set at 0%. Snow losses were not considered. An isotropic sky model was used.

3) *Calibrate the modeled energy data against the actual energy data*. A linear fit of uncalibrated modeled versus actual data was used to generate a calibration curve. The calibration curve transformed the uncalibrated data such that there will be a slope of 1 when the calibrated modeled generation data is plotted against the actual generation data. Only data that were not affected by snow were considered for the calibration curve. These data were identified as those days where the snow depth on the ground, and the snowfall, was zero. In Canada, snowfall and snow depth data is available from Environment Canada.

4) *Clean the actual energy generation data*. Actual energy data was sometimes missing. This data was flagged and replaced with calibrated model data. Where replacement was necessary, it was always done across all modules. Missing data is summarized in Table 1 both for the entire year and for days that would likely have been affected by snow losses. Missing data from 2016 and 2017 is significant. Between a quarter to a third of the data is missing when there was snow on the ground. These days could have had snow losses, but those losses could not be included in the calculation.

5) *Determine the baseline standard deviation* (σ) *of the modeling error in the absence of snow*. The modeling error is the calibrated modeled energy subtracted by the actual energy. Baseline data unaffected by snow was selected as in Step 3). Baseline data from one module pair is shown in Figure 4.

6) *Use σ to identify outlier data points*. See Figure 5 and 6. Any day where the modeled energy was $+3\sigma$ away from the calibration line was suspected of snow losses. About 0 kWh actual energy generation, $+2\sigma$ was used as the threshold. This was done based on the data visualization which suggested that the $+3\sigma$ filter was missing days affected by snow near 0 kWh actual energy generation.

7) *Total the modeling error* for all the points identified in Step 6. This is the estimated energy lost due to snow.

Table 1. Days with Missing Data

Year	*Total Days Missing From Year*	*Total Days Missing When Snow Depth > 0 cm*	*Total Days with Snow Depth > 0 cm*
2011	31	5	70
2012	0	0	30
2013	9	9	97
2014	0	0	95
2015	0	0	64
2016	32	22	68
2017	41	20	59

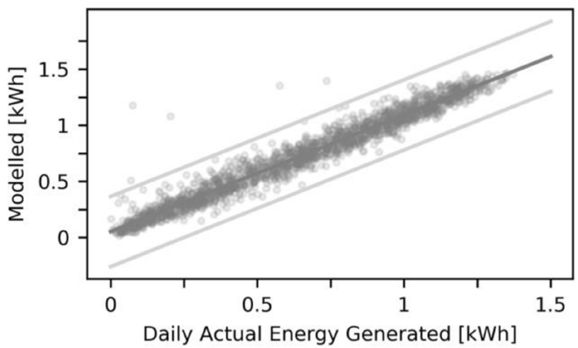

Figure 4. The baseline standard deviation of the modeling error is determined using data that is unaffected by snow—i.e. when there was no snowfall or no snow on the ground. The data in this plot are for a 0° tilt. The light grey lines represent ±3σ.

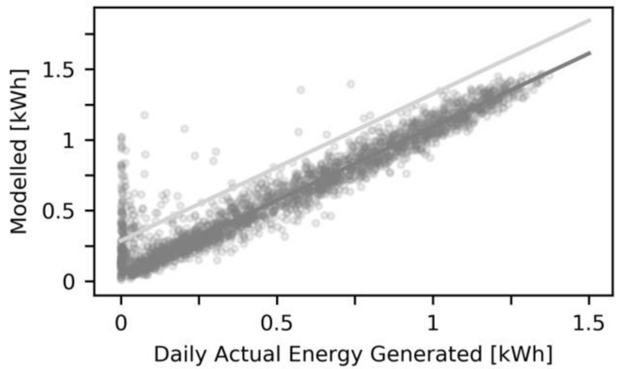

Figure 5. Days affected by snow have a modeled energy that is much greater than the actual energy. These days can be identified by the modeling error, which is greater than a threshold value determined from the baseline standard deviation (light grey line represents +3σ). The data in this plot is for a 0° tilt.

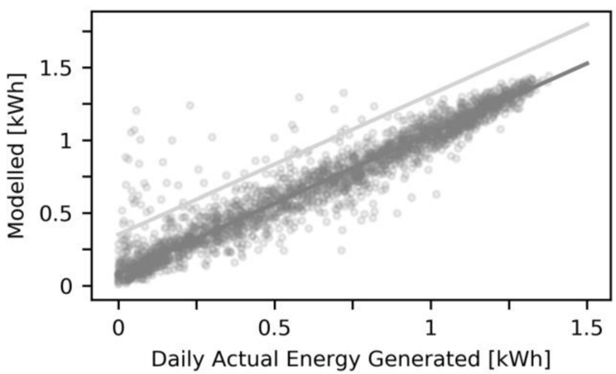

Figure 6. The data in this plot is for the 30° tilt. As expected, there are fewer outliers, and therefore lower snow losses, when compared to Figure 5. Note that the data points where the actual energy is notably greater than the modeled energy may be related to albedo, which was not considered in detail within the modeling.

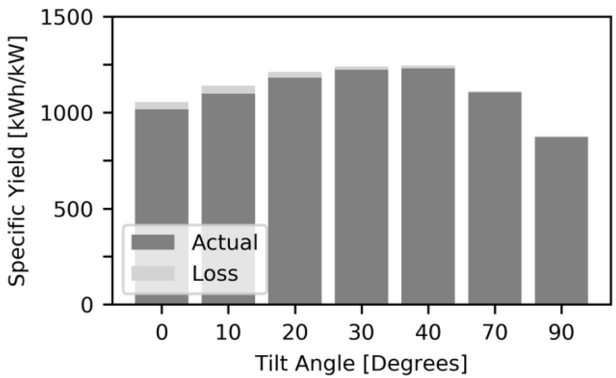

Figure 7. Mean annual yield and estimated losses from 2011 to 2017. Losses decrease with increases tilt.

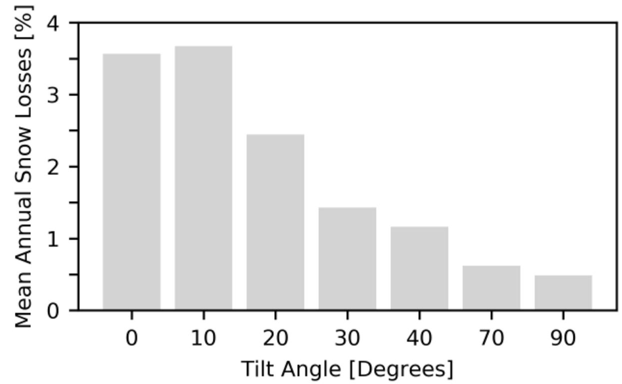

Figure 8. The mean annual estimated snow loss decreases with increasing tilt angle.

Table 2. Annual Summary of Measured Yield (kWh/kW) and Estimated Snow Losses (%) (Losses in Brackets)

Year	*0°-Pole*	*10°-Pole*	*20°-Pole*	*30°-Pole*	*40°-Pole*	*70°-Pole*	*90°-Pole*	*Roof Port.*	*Roof Lan.*	*Ballasted*
2011	992 (3)	1079 (4)	1143 (3)	1196 (2)	1190 (2)	1083 (2)	862 (1)	1164 (6)	1179 (6)	1175 (7)
2012	1095 (0)	1177 (0)	1225 (0)	1260 (0)	1246 (0)	1084 (0)	810 (0)	1305 (1)	1322 (1)	1321 (1)
2013	1030 (3)	1114 (3)	1185 (3)	1218 (3)	1229 (2)	1105 (1)	877 (0)	1191 (8)	1202 (8)	1267 (5)
2014	972 (6)	1043 (7)	1147 (4)	1198 (2)	1217 (1)	1117 (0)	903 (0)	1186 (8)	1196 (8)	1182 (10)
2015	1022 (9)	1117 (7)	1226 (4)	1284 (3)	1302 (2)	1184 (1)	951 (1)	1291 (9)	1295 (10)	1281 (10)
2016	1076 (2)	1137 (3)	1247 (1)	1278 (0)	1279 (0)	1135 (0)	887 (1)	1317 (3)	1359 (3)	1287 (4)
2017	931 (1)	1022 (2)	1103 (1)	1132 (1)	1146 (0)	1021 (0)	810 (0)	1179 (2)	1223 (2)	1163 (3)

There are two main benefits to this approach. Firstly, high accuracy is not required for the modeling component of the algorithm because it only needs to identify days affected by snow, and it is calibrated against actual data using a simple linear fit in Step 3). Secondly, there is confidence that the calculated energy lost is, in fact, largely due to snow and not some other modeling error since only those days with a very large error were considered. The main drawback is that there may be days with a small amount of energy loss due to snow that were not identified as outliers and not included in the loss calculation. Note that there were no shading objects at the STEP PV Test Lab. Installations with significant shading would need to take this into account within the modeling.

RESULTS

Pole-mounted modules

The mean specific yield (i.e. the ratio annual kWh energy yield over the kW rating of the array), and estimated losses, from each of the pole-mounted module pairs over the study period is shown in Figure 7 and Table 2. Losses are also presented in Figure 8. As expected, losses decrease with increasing tilt. Differences in the specific yield and snow losses between the 40° portrait and landscape modules were <1% and comparable to the other module pairs where both were mounted in portrait orientation.

The authors note that pole mounting of modules as has been done in this study is not a common configuration for ground-mounted installations. It was used in this case as an experimentally-expedient way of incorporating ground mounted modules at different tilt angles. A larger ground-mounted array on conventional racking with a tilt angle of 30° was adjacent to the other arrays. Power production data for this array was not available. However, image data suggests approximately comparable snow coverage between the pole-mounted and conventional rack-mounted modules (Figure 9).

The annual snow losses correlate approximately with the sum of daily snow depths for the year (Figure 10; snow data in Table 3 is from Environment Canada). This variable was identified in [1] and is defined in Equation 1, where D_{annual} is the annual sum of daily snow depths and D_i is the snow depth on any given day indexed by the subscript i. The variable incorporates snowfall amounts but also indirectly incorporates other important variables like temperature.

$$D_{annual} = \sum_{i=1}^{365} D_i \qquad \text{Eq. 1}$$

Modules on Roof-Section and Flat Deck

The mean specific yield and estimated snow losses for the modules mounted on the roof section and flat deck are shown in Figure 11 and 12. Annual values are in Table 2. Annual losses vary from 0% to as much as 10%. The specific yields of the roof-mount and ballasted modules are higher than the corresponding pole-mounts. This is because the modules are newer and in a better state of repair. Losses are much greater than the corresponding pole-mounted modules.

The poorer snow-shedding of the roof-mounted arrays was also evident from image data. Figure 9 shows the 0°, 10°, and 20° pole-mounted modules

Figure 9. (Left) Pictures taken at noon over 4 consecutive days from Jan 16th to Jan 19th, 2014 (from top to bottom), of the 20°, 10° and 0° pole-mount arrays (from left to right), as well as the roof-mounted and ballasted array. It's clear that the 20° pole-mounted array (the left-most pole-mounted modules) is shedding snow much better than the roof modules which are at a lower tilt. The images also show a larger roof-mounted array that remained covered in snow. Records of this array are not available, but it is believed to have not been operating while these pictures were taken.

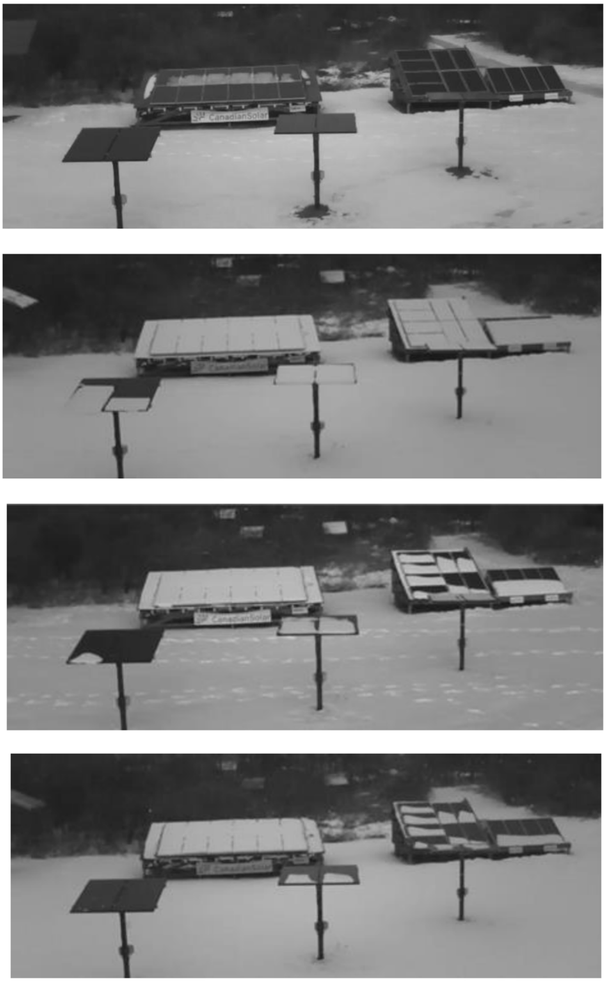

as well as the 30° roof section and 37° ballasted modules at noon over 4 consecutive days. The 20° pole-mounted module is fully free of snow much sooner that the 30° roof section modules and 37° ballasted modules. The issue is that snow accumulates at the bottom frame of these modules and does not shed easily. On the ballasted modules, there is a flat ledge upon which snow can accumulate and prevent melting snow from fully shedding (as would happen in an actual installation mounted on a flat roof). There were no significant differences between the portrait and landscape modules, similar to the 40° pole-mounted modules.

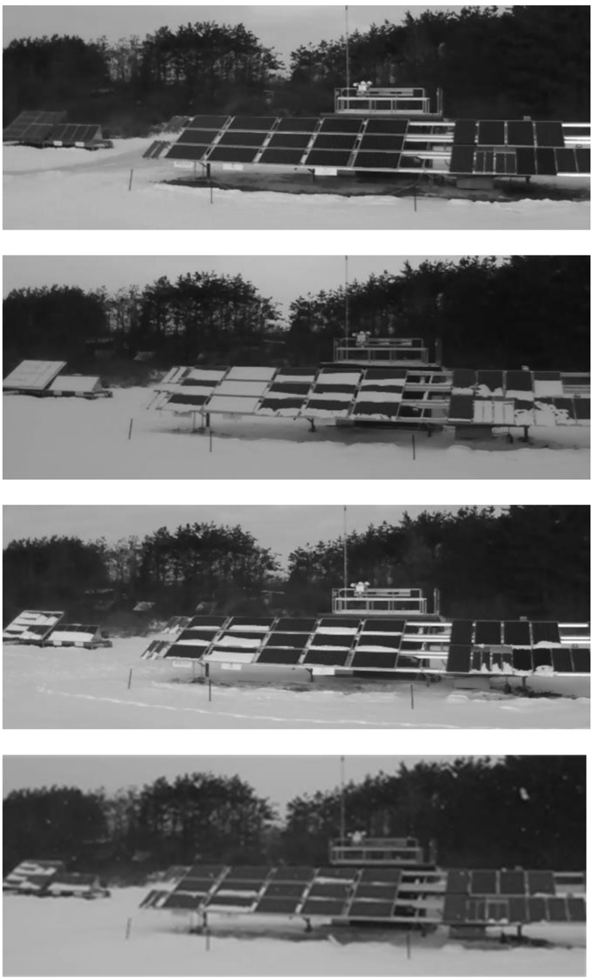

(Right) A larger ground-mounted array installed on more conventional racking at a 30° tilt is shown at the same time of day and covering the same time period. Data were not available for the modules on this array, but the image data suggest comparable (or better) snow-shedding behaviour to the 20° pole-mounted module.

Table 3. Snow Data.

Year	*Total Snow [cm]*	*Annual Sum of Daily Snow Depths [cm]*	*Max Snow Depth [cm]*
2011	155	922	35
2012	105	143	14
2013	180	1074	37
2014	176	1883	38
2015	90	855	28
2016	163	506	25
2017	109	356	20

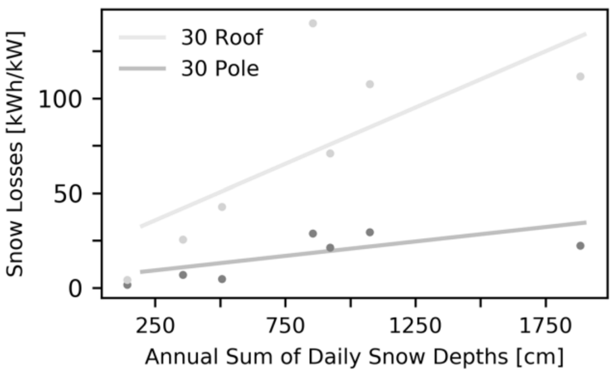

Figure 10. As an example, annual losses for the 30° pole- and roof-mounted modules correlate with the sum of daily snow depths (R2 of 0.52 and 0.63, respectively).

Procedure Applied to Freely Available Datasets

Another important strength of this method for estimating snow losses is that it can be applied to freely available PV generation datasets, of which there are many. This can aid in overall efforts to validate snow loss models. For example, Enphase allows system owners the option of making a subset of their PV system performance data viewable to the public. The public sites also typically provide system information like module model, tilt, and azimuthal orientation. This is enough information for a system model that can be used to estimate snow losses. This section provides a concrete example of the calculation procedure applied to a freely available PV generation dataset.

A publicly viewable Enphase PV installation with system ID GSMz94049 was found via internet search. It is a residential system located in Calgary, Alberta, Canada, and was installed in July 2012. It consists of 1 array with 12 modules. The tilt is 18.4° and the azimuthal orientation is 180° (due South). Modules models were CS6P-215PE from Canadian Solar. A precise address was not provided, nor were any pictures of the installation. The presence of any shading objects was determined by investigating the shape of the daily generation curve for clear-sky days near the winter solstice and spring equinox—again, these data were freely available from the public view of the instal-

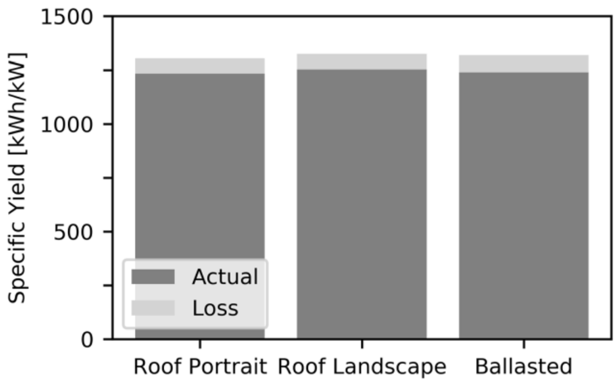

Figure 11. The mean annual snow losses are greater for the modules mounted on the roof section and ballasted on the flat deck, when compared to the pole-mounted modules (Figure 7).

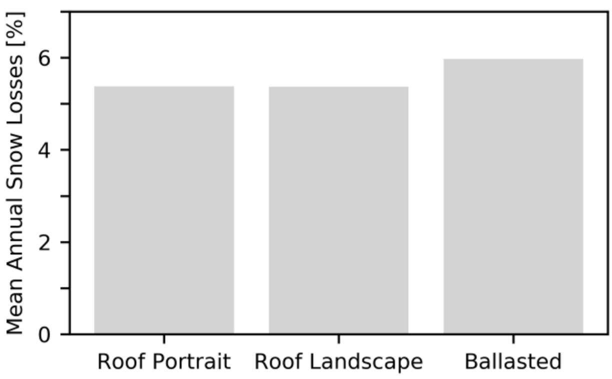

Figure 12. Mean annual snow losses are between 5 and 6% for the arrays mounted on the roof-section and ballasted on the flat deck. The landscape and portrait modules mounted on the roof section had comparable performance.

lation. The daily energy generation profile for different clear-sky days is shown in Figure 13. The symmetry and shape show that there is no significant shading—and it follows that any outlying data points in the modeling are not attributable to shading objects.

Daily energy generation for 2013 to 2017 was collected from the public view of the installation accessible online. A SAM model was created using the available system information and environmental data from NSRDB. A constant albedo was assumed. An isotropic sky model was used. All losses were set to 0%. The daily actual energy generation versus uncalibrated modeled data is shown in Figure 14. The figure also shows a linear calibration curve created by considering only those points from June, July and August. All modeled data were then adjusted by the calibration curve. The modeling error using data from June, July and August, was used to determine the baseline standard deviation of the modeling error in the absence of any snow. A maximum modeling error of $+3\sigma$ was used to identifying outlying data points.

The modeling error of points above the threshold was then aggregated to estimate the total energy lost due to snow. The annual actual generation and estimated losses is shown in Figure 15. The annual sum of daily snow depths for this installation had a relatively narrow range and was not well correlated with total annual energy loss due to snow.

DISCUSSION

This article has suggested a simple empirical approach to estimating snow losses based on daily energy generation data that is often available for PV systems. It requires no extra sensors and uses freely available tools (SAM) and environmental datasets (NSRDB). The modeling component is simple and only requires a few system parameters. The additional analysis is straightforward to perform in standard spreadsheet software package. It could therefore be performed by PV system owners with minimal modeling experience. Empirical data on snow losses is useful to system owners for a variety of reasons. For example, it can quantify the lost revenue, inform decision-making around snow removal, help explain shortfalls and variations in energy yield, and help inform energy consumption targets for buildings seeking net-zero energy.

The analysis of the various PV arrays at the STEP PV Test Lab demonstrates the effectiveness of the method. The analysis has shown very clearly that when the only days considered have no snow on the ground or no snowfall, the agreement between modeled and actual generation follows a very tight

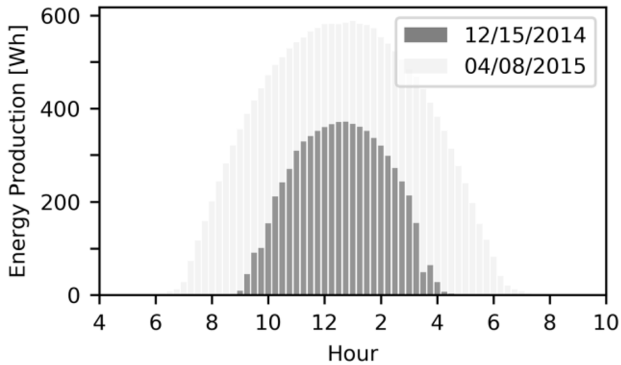

Figure 13. The symmetry of the generation curve for clear-sky days near the winter solstice and spring equinox shows that there is no significant shading for this installation. However, there does appear to be a small shading object in the western sky that has a small impact when the sun is at its lowest elevation.

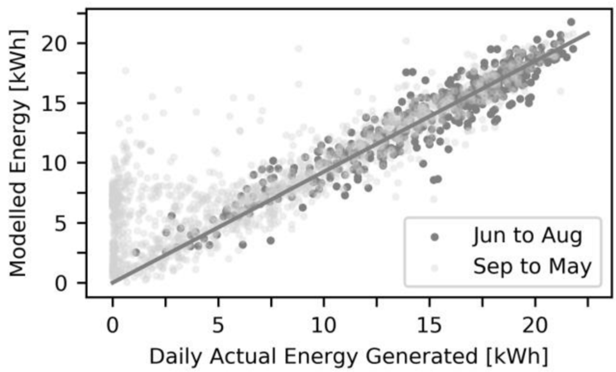

Figure 14. The uncalibrated modeled data are shown for 2013 to 2017 and have been separated into days occurring in June to August and days occurring in the rest of the year. It's clear that the statistical spread of the summer data, with no presence of snow, is lower than when compared to that for the rest of the year.

distribution (this was shown in Figure 4). When data that may have been affected by snow is included, obvious signatures (Figure 5) show up that can be isolated and quantified based on the baseline standard deviation of the modeling error. Furthermore, the expected trends occur when the method is applied to increasing tilt angles, with the losses being greatest for the lowest tilts. It was also shown that the losses estimated using this approach correlate with snow data. These observations all support the validity of the approach.

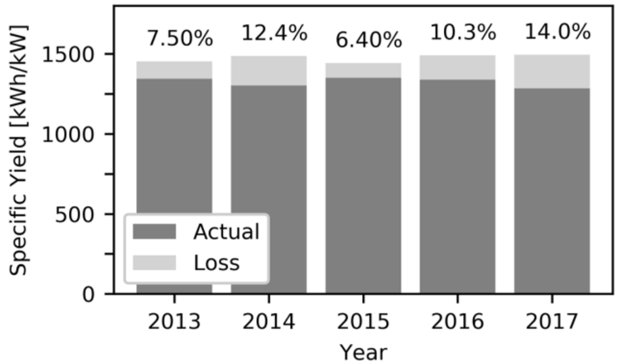

Figure 15. The actual energy generation and estimated losses from snow coverage are shown for each year that data was available. This plot demonstrates that it is possible to estimate snow losses using freely available datasets, relatively few parameters and a simple system model.

It's important to note that the research team had no affiliation with the publicly viewable Enphase site in Calgary. All the data and tools used to estimate snow losses were freely available online. Continuing to use Enphase as an example, this is only one of many sites and it is straightforward to see how this basic approach could be used to estimate snow losses of PV systems across the Northern U.S. and Canada by using actual system energy production data. A map of Enphase installations is available in [8]—it claims more than 895,000 installations. A small subset of these are publicly accessible. That data can be used to generate an experimental map of PV system snow losses across different geographical areas, years, and system types, based on the simple approach outlined in this article. It follows that the generation of snow loss estimates and validation of snow loss models using real-world data across a large number of sites covering different geographical regions should be feasible without significant effort obtaining experimental data.

CONCLUSION

This study presented measured yield and estimated snow loss data spanning from 2011 to 2017 from PV arrays mounted at several different tilt angles, also considering pole and roof-mounting styles. It found that the greatest snow losses in any particular year (10%) occurred for the roof-mounted modules and the modules mounted with ballast on the flat deck. The data is useful for snow loss estimates in the immediate geographical area of the study. The range of tilt angle and mounting styles considered also makes the dataset useful for snow loss model validation efforts. This study also showed that the approach used to estimate snow losses could easily be applied to other installations using typically available system data and free software tools. This makes empirical estimates of snow losses more accessible to a broader number of PV system owners. Such estimates can be used can monetize the energy loss, inform decision-making around snow removal, help explain shortfalls and variations in energy yield, and help inform energy consumption targets for buildings seeking net-zero energy consumption.

Acknowledgements

Base funding for STEP low-carbon technology evaluations is provided by the Region of Peel, York Region and The City of Toronto. Financial support for STEP's PV Test Lab has been provided by Natural Resources Canada. Note that the contents of this article do not necessarily represent the policies of the supporting agencies. Although every reasonable effort has been made to ensure the integrity of the article, the supporting agencies do not make any warranty or representation, expressed or implied, with respect to the accuracy or completeness of the information contained herein. Mention of trade names or commercial products does not constitute endorsement or recommendation of those products.

References

[1] D. S. Ryberg, and J. Freeman. "Integration, validation, and application of a PV snow coverage model in SAM," NREL Technical Report TP-6A20-68705, 2017.

[2] R. Andrews and J. Pearce. "Prediction of energy effects on photovoltaic systems due to snowfall events," in 38th IEEE Photovoltaic Specialist Conference, pp. 3386-3391, 2012.

[3] B. Marion, R. Schaefer, H. Caine, and G. Sanchez. "Measured and modeled photovoltaic system energy losses from snow for Colorado and Wisconsin locations," Solar Energy, vol. 97, pp. 112-121, 2013.

[4] L. Powers, J. Newmiller, and T. Townsend. "Measuring and modeling the effect of snow on photovoltaic system performance," in 36th IEEE Photovoltaic Specialist Conference, pp. 973-978, 2010.

[5] T. Townsend and L. Powers. "Photovoltaics and snow: An update from two winters of measurements in the SIERRA," in 37th IEEE Photovoltaic Specialist Conference, pp. 3231-3236, 2011.

[6] Northern Alberta Institute of Technology Alternative Energy Program. "Solar photovoltaic reference array report." March 2016. Accessed online July 2019: solaralberta.ca/sites/default/files/NAIT%20Reference%20Array%20Report.pdf.

[7] N. Heidari, J. Gwamuri, T. Townsend and J. Pearce. "Impact of snow and ground interference on photovoltaic electric system performance," IEEE Journal of Photovoltaics, vol. 5, issue 6, 1680-1685, 2015.

[8] Enphase Installation Map. Accessed online May 2019: enphase.com/en-us/map.

ABOUT THE AUTHORS

Erik Janssen is an analyst with the Sustainable Technologies Evaluation Program (STEP) of the Toronto and Region Conservation Authority (TRCA). For several years he has been a scientific lead on STEP pilot projects evaluating emerging low-carbon energy technologies. He is a CMVP and holds an M.A.Sc. in Engineering Physics, a Swedish Magisterexamen in Solar Energy Engineering and a B.Sc.(Hon) in Physics. Email: erik.janssen@trca.ca

David Nixon is an advisor to STEP and his experience with renewable energy spans more than 20 years, including the installation of on- and off-grid wind and PV systems, residential and commercial solar hot water systems, the design and manufacturing solar electric equipment, and device-level research in a laboratory setting.

Svend De Bruyn is a Renewable Energy Specialist with more than 10 years at STEP. He has 25 years experience in the PV and wind industries regarding sales, service, and installation. He has been a consultant for the Canadian Wind Energy Association and an instructor at Durham College.

Gil Amdurski is Technical Coordinator with STEP, specializing in the instrumentation of renewable energy systems. He holds a Diploma in Electromechanical Engineering, a Post-Graduate Certificate in Renewable Energies, and is Certified Measurement and Verification Professional with the Association of Energy Engineers.

Leigh St. Hilaire is a Project Manager with STEP, where he has managed a diverse set of energy-related research projects. Prior to STEP, Leigh worked for Exova, where he was responsible for designing, procuring, certifying and deploying a PV testing laboratory. Leigh holds a B.A.Sc in Electrical Power System Engineering.

Guidelines for Submittals

The *Alternative Energy and Distributed Generation Journal* (AE&DG) is a bimonthly publication of the Association of Energy Engineers, Atlanta, GA, USA. The journal invites original manuscripts involving analytical engineering, management, strategy and/or policy approaches to distributed generation, cogeneration, combined heat and power, alternative energy (from renewable and non-renewable sources) and related systems. We accept both original research and development work, novel case studies and significant design/analysis efforts. Generally, design work is that which specifies a new system, process or product. Analysis highlights modifications, retrofit or improvements carried out on an existing system, process or product.

Manuscript Preparation

We prefer your copy be produced in MsWord. If this software is not available to you, the text should be saved in rich text format or ASCII format (w/line breaks). Please note the following submission requirements:

- Use the New Times Roman 12 and Symbols fonts. Use of other fonts (especially Cambria Math) can cause your submission to be rejected.

- Major subject headers should be in all caps; secondary headers in bold caps & lower case; subsequent headers in medium italics.

- Indent at the beginning of each new paragraph. Please single space your article.

- Please do not use an automatic reference or footnote format. When you need to insert a footnote or reference number, just type it in brackets, i.e., [XX], or [X-XX] as applicable.

- Please do not use an automatic outlining or bullet format. TYPE IN your numbers, bullets, and letters, and just tab after them. Automatic formats "fall out" when the document is moved into a page-layout program such as InDesign, so just don't use them.

- Equations must be in perfect order and capable of high resolution when converted to PDF formats. Do not use imported equations from menus in MsWord.

- When using an acronym such as VSD, spell out its first occurrence in your text; e.g., "variable speed drive (VSD)." Capitalize only the acronym (unless using a proper name).

When submitting your article, also include a PDF copy in your email. All graphics must of high resolution (400-600 dpi).

Title: The title should express the main point of the article and list the full names of all authors below.

Abstract: An abstract at the beginning should summarize the article and highlight significant new information and conclusions.

Introduction: The introduction should outline the issue, its significance, and how it is approached in the main body of the manuscript.

Main Body of Manuscript: This section develops the thought of the article. A good article normally presents the results with text, tables, and perhaps illustrations.

Conclusions: A summary should state conclusions, final comments, and any necessary qualifications. Suggestions for further research might be appropriate here.

References: A bibliography should list all references in order of appearance in the text. References usually show author name, title of article/book, publishing company, location and date. Do not abbreviate journal names in the references. Remove underscores, hyperlinks, and italics when web addresses are used and note website access dates (e.g., http://www.somewebsite.com, accessed 25 May 2018). Example of reference formatting:

[1] Mendis, N. and Perera, N. (2006). Energy audit: a case study. Information and Automation, pages 45-50.

Appendix: Appendices, if used, should present supporting data not given in the body, or materials which are too detailed to include in the body. For example, spreadsheet calculations require too much space in the body of the manuscript. Alternatively, the author might show one set of calculations in the body and present the spreadsheet in the appendix.

Figures and Tables: All artwork should be in tiff format and of at least 400 dpi resolution, with captions and with numbering when needed. Avoid low-resolution images, such as screen captures. A better strategy would be to make textual reference to the information and let readers check the site. Multi-color charts and graphs are unsuitable as our publications are in black and white.

Verification and Validation: When the published research, design or analysis work entails and includes the development or application of new simulation models of complex or complicated systems, products or processes, we require the Verification and Validation (V&V) of such simulation models. Verification is making sure all data and analyses are numerically correct and accurate. Validation is assuring the underlying simulation model(s) are truly representative of the actual or real system, product or process being modeled, with enough accuracy.

Author Biography: Provide a brief biographical section stating the author's affiliation and a background description. If there is one author, this section must be less than 75 words. For more than one author, no more than 50 words per author. State how a reader might contact the author (email is preferred).

Peer review means the editor will send the article to two or three reviewers after initial editing and request review and comments. Typically, reviewers ask for changes or responses to questions prior to their approval for publication. Once they give approval, the editor will publish the article and show peer reviewed above the title. This process may add six months or more to the lead time for publication. Peer reviewed author(s) will need to respond to multiple reviews and may need to verify the typeset proof of the article prior to publication.

A statement should be included in your cover letter transferring copyrights for the article to the Association of Energy Engineers. If you have need of a sample article to aid in understanding our formatting requirements please contact the editor and one will be provided. Any questions should be addressed to:

Dr. Jorge B. Wong
Editor-in-Chief
The Alternative Energy & Distributed Generation Journal
8 Dawn Meadow Ct.
Simpsonville, SC 29680
USA
jwong@aeecenter.org

About this Journal

The Alternative Energy and Distributed Generation Journal is an official quarterly publication for members of the Association of Energy Engineers. The journal publishes original articles and papers addressing state-of-the-art technological advances in cogeneration and distributed generation, solar, wind, biomass, and other green, renewable, and alternative energy sources.

Published by the Association of Energy Engineers

Over 18,000 professionals in 105 countries trust the Association of Energy Engineers (AEE) to promote the interests of those engaged in the energy industry and to foster action for sustainable development. Our members operate in the dynamic fields of energy engineering, energy management, renewable and alternative energy, power generation, energy services, sustainability, and all related areas.

aeecenter.org